Fissility of preactinides in charged-particle induced reactions

A. V. Ignatyuk and G. N. Smirenkin

Physics and Power Institute, Obninsk

M. G. Itkis, S. I. Mul'gin, and V. N. Okolovich

Institute of Nuclear Physics, Kazakh Academy of Sciences, Alma-Ata

Fiz. Elem. Chastits At. Yadra **16**, 709–772 (July–August 1985)

The main results of investigations of the integrated and differential cross sections of fission by light charged particles in the region of nuclear masses $170 \lesssim A \lesssim 215$ are reviewed. The available experimental data on the energy dependence of the preactinide fissilities are analyzed in the framework of a statistical approach based on description of the level density in the superfluid nuclear model with phenomenological allowance for shell and collective effects. It is shown that the new experimental information on the heights of the fission barriers requires revision of the parameters in the isospin dependence in the existing variants of the liquid-drop model. The directions of further investigations needed for an adequate description of the nuclear masses and deformation energies are discussed.

INTRODUCTION

Although the pioneering ideas about fission probability were formulated by Bohr and Wheeler[1] very soon after the discovery of the phenomenon itself, the experimental study and development of methods of theoretical description of fission probability remain among the most topical problems even now, more than 40 years after the original discovery. Measured by the rate of development of modern science and the intensity of research in the field, this is a very long period of time, indicating the magnitude of the difficulties that have been and are still encountered in fission physics.

In the fission process, a most important part is played by the potential barrier that keeps a heavy nucleus from the energetically advantageous breakup into parts. It determines many properties of the nuclei—from stability with respect to spontaneous fission, which delineates the boundaries of the periodic system, to the probability of induced fission, knowledge of which is of great practical importance for the exploitation of fission as a source of nuclear energy.

Practical applications and related branches of nuclear physics impose high requirements on the description of the barrier and the fission probability determined by it, but at the present time theory cannot meet these requirements, although the foundation of theory is the liquid-drop model of the nucleus, which has a history of more than half a century. Intensive searches are still being made for the most adequate variant of this model, since the absence of clarity in this question is one of the main sources of uncertainty in theoretical predictions. The reliability of the experimental information on the drop component of the barrier increases with decreasing Z in accordance with the increase in its contribution to the deformation potential energy of the fissioning nucleus. This is one of the reasons why the study of the fission of preactinides, which are outside the region $Z \geqslant 90$ of nuclei of greatest interest for practical purposes, attracts considerable interest and plays an important part in forming ideas about the fission barrier.

The raising of the fission barrier on the transition from the actinides to the preactinides plays a dual role. On the one hand, the raising of the barrier extends the region of energies in which emission fission preceded by neutron emission, which is the main difficulty in studying the fission of highly excited heavy nuclei, makes a small contribution. On the other hand, the increase in the barrier decreases the fission probability exponentially, and this strongly hinders its experimental study. In particular, the fission threshold, which is readily established in the case of the actinides from the region of the sharp "bend" in the fissility, is accessible in the preactinides, their fission probability being low, only for a small group of nuclei in the immediate vicinity of lead. The main method used to determine the barrier height E_f for the lighter nuclei is by analysis of the experimental data on the fissility in the above-barrier region of energies by means of a statistical description.

Although E_f is a parameter with respect to which the statistical description is very sensitive, the isotopic dependence $E_f(Z,N)$ can be investigated with sufficiently high accuracy only if correct allowance is made for numerous factors that affect the probability of the fission process. They include not only the properties and parameters of the potential energy at large deformations, i.e., in the *transitional* state (or, in other words, at the saddle point) of the fissioning nucleus, which determine the fission channel of the reaction, but also the characteristics of the nuclei in the ordinary equilibrium state that determine the neutron channel of the reaction, which is responsible for the main competing process—neutron emission.

The study of the preactinides is of interest not only on account of the very large deformations of the transitional states of the nuclei but also because of the remarkable variety of properties of the ground states. The region of the preactinides includes not only islands of the greatest stability of spherical nuclei in the neighborhood of the doubly magic ^{208}Pb but also a large group of strongly deformed nuclei with $Z \lesssim 76$. As a result of this, the fission of the preactinides is a very important source of experimental information about the part played by shell and collective effects—a topical

 0090-4759/85/040307-30$04.40

problem in the statistical description of the properties of strongly excited nuclei.

Questions that arise in the study of preactinide fission have been the subject of a series of studies by a collaboration between the Institute of Nuclear Physics of the Kazakh Academy of Sciences and the Physics and Power Institute during the last ten years. This collaboration has, on the one hand, greatly enriched the experimental data on fissility and, on the other, led to the development of an approach to its analysis in which the currently most complete allowance is made for the details of the formation of the compound system and the statistical properties of the excited nuclei that determine the various decay channels.

The present review summarizes the results of the investigations. It analyzes all the available experimental information on the energy dependence of the fissility of the preactinide nuclei obtained in reactions with light charged particles, $A \leqslant 4$, and electrons at energies of the projectiles up to 80 MeV. If higher particle energies or heavier ions are used, the greater complexity of the reaction mechanisms greatly increases the uncertainty of the extracted information about the fission barriers and the other characteristics of the transitional states of the fissioning nuclei.

1. STATISTICAL DESCRIPTION OF INTEGRATED AND DIFFERENTIAL FISSION CROSS SECTIONS

In accordance with the general ideas of the model of the compound nucleus, the relations for the integrated fission cross sections can be written in the form[2,3]

$$\sigma_f(E_i) = \pi\lambda_i^2 \sum_J g_J T_J(E_i) \frac{\Gamma_f^J}{\Gamma_f^J + \sum_{i'} \Gamma_{i'}^J}, \tag{1}$$

where λ_i is the wavelength of the incident particle with energy E_i, $g_J = (2J+1)/(2S_i+1)(2I_0+1)$ is the statistical factor determined by the spin S_i of the particle, the spin I_0 of the target nucleus, and the angular momentum J of the compound nucleus, T_J are the penetrabilities, Γ_f^J is the fission width for fixed J, and $\Gamma_{i'}^J$, are the decay widths that compete with the fission. In the majority of cases, it is more convenient to analyze, not the fission cross sections, but the fissility (the fission probability), which is determined by

$$P_f = \frac{\sigma_f(E_i)}{\sigma_c(E_i)} = \sum_J P_f^J \sigma_c^J(E_i)/\sigma_c(E_i), \tag{2}$$

where σ_c^J is the cross section for the formation of a compound nucleus for fixed angular momentum, and $\sigma_c = \Sigma_J \sigma_c^J$ is the total cross section for formation of a compound nucleus. The fissility depends much less strongly on the characteristics of the projectile than the fission cross section, and this circumstance is very favorable for comparing experimental data having heterogeneous methods of excitation.

The number of parameters that characterize the various widths is significantly reduced in the above-barrier region, in which a statistical description of the number of open channels can be used. In this case, the fissility is determined by competition between the two dominant widths—the fission and neutron widths. The dependence of the widths on the excitation energy and on the angular momentum can be represented in the form[2,3]

$$\left.\begin{aligned} \Gamma_f^J(E) &= \frac{1}{2\pi\rho_c(E,J)} \int_0^{E-E_f} \rho_f(U,J)\,dU, \\ \Gamma_n^J(E) &= \frac{A^{2/3}}{\pi\varkappa\rho_c(E,J)} \int_0^{E-B_n} \rho_n(U,J)(E-B_n-U)\,dU, \end{aligned}\right\} \tag{3}$$

where E_f is the height of the fission barrier, B_n is the neutron binding energy, $\varkappa = \hbar^2/2\mu r_0^2 \simeq 10$ MeV, $\rho(U,J)$ is the level density of the excited nucleus, and the indices c,f,n identify the compound nucleus and the fission and neutron channels, respectively.

As was shown by Bohr,[4] one must consider as fission channels all possible transitional states of the fissioning nucleus at deformations corresponding to the top of the fission barrier. It is expected that the sequence of such states is like the observed spectra of the excited states of stable deformed nuclei. Besides the total angular momentum, the states of deformed nuclei can also be characterized by the projection K of the angular momentum onto the symmetry axis of the nuclei. For the transitional states of fissioning nuclei, the direction of separation of the fragments is a symmetry axis, and the density of the transitional states can be represented in the framework of the statistical approach in the form

$$\rho_f(U,J) = \frac{\rho_f(U)}{2\sqrt{2\pi}\sigma_\parallel} \sum_{K=-J}^{J} \exp\left\{-\frac{J(J+1)}{2\sigma_\perp^2} - \frac{K^2}{2\sigma_{\text{eff}}^2}\right\}, \tag{4}$$

where $\rho_f(U)$ is the total density of the excited states and $\sigma_j^2 = \mathcal{J}_j t/\hbar^2$ are the parameters of the spin dependence of the level density, determined by the temperature t of the excited nucleus and the perpendicular, $\mathcal{J}_\perp$, parallel, $\mathcal{J}_\parallel$, or effective, $\mathcal{J}_{\text{eff}} = \mathcal{J}_\perp \mathcal{J}_\parallel/(\mathcal{J}_\perp - \mathcal{J}_\parallel)$, moment of inertia of the nucleus, respectively.

Using (4) and the analogous formula for the level density of the neutron channel, we obtain for the ratio of the fission and neutron widths

$$\frac{\Gamma_f^J}{\Gamma_n^J} = \frac{\varkappa}{2A^{2/3}} \gamma(J) \frac{\int_0^{E-E_f} \rho_f(U,0)\,dU}{\int_0^{E-B_n} (E-B_n-U)\rho_n(U,0)\,dU}. \tag{5}$$

Here, all the factors that depend on the angular momentum are separated in the factor

$$\gamma(J) = \frac{\sqrt{2\pi}K_0}{2J+1} \exp\left[\beta(J+1/2)^2\right] \operatorname{erf}\left(\frac{J+1/2}{\sqrt{2}K_0}\right), \tag{6}$$

$$K_0 = \sigma_{\text{eff}}^{(f)}, \quad \beta = \frac{1}{2}(\sigma_{\perp n}^{-2} - \sigma_{\perp f}^{-2}).$$

It should be noted that when the spin factors are separated in (5) the parameters σ_i^2 are taken in front of the integral in accordance with the mean-value theorem. Therefore, their argument is not the maximal excitation energy of the nucleus in the corresponding channel but a somewhat lower value. However, since the integrands depend exponentially on the excitation energy, these differences are, as a rule, ignored.

To determine the penetrabilities $T_J(E_i)$ and the cross sections $\sigma_c(E_i)$ for formation of a compound nucleus, the

optical model is usually used. Simplifying somewhat the description of the distribution of the angular momenta in the compound nucleus, one can use the semiclassical estimate for the penetrabilities:

$$T_J = \begin{cases} 1 & \text{for } J \leqslant J_{\max}; \\ 0 & \text{for } J > J_{\max}. \end{cases} \tag{7}$$

In this case, it is expedient to determine the maximal angular momentum $J_{\max}$ on the basis of optical calculations:

$$J^2_{\max} = 2\sum_J (2J+1)\, T_J J(J+1) / \sum_J (2J+1)\, T_J = 2\langle J^2\rangle_{\text{opt}}. \tag{8}$$

In the semiclassical approximation in the region of excitation energies in which the contribution of fission preceded by neutron emission can be ignored, the fissility of the pre actinides can be described by

$$\left.\begin{aligned} P_f(E) &= \frac{\Gamma_f^0}{\Gamma_n^0}\,\bar{\gamma}(J_{\max}), \\ \bar{\gamma}(J_{\max}) &= J_{\max}^{-2}\int_0^{J_{\max}} (2J+1)\,\gamma(J)\,dJ, \end{aligned}\right\} \tag{9}$$

where Γ_f^0/Γ_n^0 is the ratio of the widths for zero angular momentum.

If the excitation energy of the compound nucleus is above the threshold of the reaction (i,nf), then not only the original nucleus A will contribute to the measured fission cross sections, but also fission of the nucleus A–1 formed after neutron emission. With further increase in the energy E, ever lighter isotopes of the initial state of the nucleus will contribute to the observed emission fissility. The emission of charged particles being effectively negligible on account of the Coulomb barrier, the resultant fissility can be represented in the form

$$\begin{aligned} P_f^{\text{obs}}(A,\ E) &= P_f(A,\ E) \\ &+ J_{\max}^{-2}\int_0^{J_{\max}} (2J+1)\,dJ \sum_{\nu=1}^{\nu_{\max}} \int_{E_f^{A-\nu}}^{E_\nu^{\max}} P_f^J(A-\nu,\ E_\nu) \\ &\times N(E_\nu)\prod_{k=0}^{\nu-1}[1-P_f^J(A-K,\ E_k)]\,dE_\nu, \end{aligned} \tag{10}$$

where $P_f(A_\nu,E_\nu)$ are the fissilities described by the relations (5) or (9), $N(E_\nu)$ is the distribution of the excitation energies in the residual nucleus after the emission of ν neutrons, and $E_\nu^{\max} = E - \Sigma_{k=1}^{\nu} B_n^{A-k+1}$. If $P_f(A_\nu,E_\nu) \ll 1$ in the complete considered energy range, then the observed fissility is approximately equal to the sum of the mean partial fissilities of all the nuclei in the emission chain of isotopes,

$$P_f^{\text{obs}}(A,\ E) \simeq \sum_{\nu=0}^{\nu_{\max}} P_f(A-\nu,\ E_\nu), \tag{11}$$

where all the terms are determined by the relation (9). From (11) there follows directly the helpful relation

$$P_f(A,\ E) = P_f^{\text{obs}}(A,\ E) - P_f^{\text{obs}}(A-1,\ E_1), \tag{12}$$

which makes it possible to extract from experimental data on the fissility of the neighboring isotopes the fissility of the initial nucleus in the region of energies in which the emission-fission contribution is important.

The relations of the compound-nucleus model for the differential fission cross sections can be written down by analogy with (1):

$$\frac{d\sigma_f}{d\Omega} = \pi\lambda_i^2 \sum_J g_J T_J(E_i)\,\frac{\sum_{|K|\leqslant J} \Gamma_f^{JK} W_{JK}(\vartheta)}{\Gamma_f^J + \sum_{i'} \Gamma_{i'}^J}, \tag{13}$$

where the function $W_{JK}(\vartheta)$ determines the angular distribution of the fragments for fixed angular momentum J and fixed projection K of it onto the direction of separation of the fragments. If the semiclassical approximation for the rotation function is used,[5] then $W_{JK}(\vartheta)$ can be represented as

$$W_{JK}(\vartheta) = \begin{cases} \frac{2J+1}{4\pi^2}\,[(J+1/2)^2\sin^2\vartheta - K^2]^{-1/2} & \text{for } \sin\vartheta > \frac{K}{J+1/2}; \\ 0 & \text{for } \sin\vartheta < \frac{K}{J+1/2}. \end{cases} \tag{14}$$

Making the same approximations as in the derivation of (9), we obtain for the angular distribution of the fragments, normalized by the integrated fissility,

$$W(\vartheta) = \frac{\sqrt{2\pi}K_0}{J_{\max}^2}\int_0^{J_{\max}} \exp\left\{\left(\beta - \frac{\sin^2\vartheta}{4K_0^2}\right)J^2\right\} I_0\left(\frac{J^2\sin^2\vartheta}{4K_0^2}\right) dJ^2, \tag{15}$$

where $I_0(x)$ is a Bessel function of imaginary argument. The expression (15) differs from the widely used Halpern–Strutinsky relations[6] only by the more rigorous allowance for the dependence of the competing decay widths of the nucleus on the angular momentum.

In the study of the differential fission cross sections, it is usual to analyze the angular anisotropy $A = W(0°)/W(90°)$ of the fragments, a relation for which can be readily obtained from the general expression (15) for the angular distribution of the fragments. For small values of the maximal angular momentum of the compound nucleus ($J^2_{\max} < 4K_0^2$), the integrands in (15) can be expanded and a simple estimate can be obtained for the angular anisotropy:

$$A \simeq 1 + \frac{J^2_{\max}}{8K_0^2} + \frac{J^4_{\max}\beta}{48K_0^2} + \dots \tag{16}$$

It is evident from this expression that measurements of the angular anisotropy of the fission make it possible to obtain information about the parameter K_0^2 or a quantity directly related to it, namely, the effective moment of inertia of the transitional states of the fissioning nuclei: $\mathcal{J}_{\text{eff}} = \hbar^2 K_0^2/t$.

2. EXPERIMENTAL INFORMATION ON FISSION PROBABILITY

Experimental investigation of the fission of the preactinides

The first systematic investigations of the fission probability of preactinide nuclei at the excitation energies in which we are interested, of the order of several tens of megaelectron-volts, were made by Fairhall, Jensen, and Neuzil[7]

by the radiochemical method—by the detection and analysis of the activity of the fission fragments produced by irradiation of the target nuclei Au, Pb, and Bi by deuterons and α particles. Their work established two of the most important features of the fission of nuclei near lead, distinguishing them from the fission of actinides: the strong dependence of the fission probability on the energy of the particles and the symmetry of the mass distribution of the fragments. The same method was used for the reaction ^{209}Bi(α, f) to determine the angular anisotropy of the fragments.[8] Subsequently, the preactinides were studied experimentally using semiconductor detectors, which made possible more detailed measurement of the integrated and differential cross sections of the (α, f) reaction[9,10] and the (d, f) reaction.[11] However, the low fission probability and high background of scattered particles made it impossible to approach closer than 5–10 MeV to the fission threshold.

A decisive factor that radically changed the experimental possibilities was the development of dielectric track detectors of the fragments almost insensitive to the background of light charged particles. The results obtained by this method determine the present state of the experimental information on the fission probability of the preactinides. The foundation was laid by the excellent studies of Refs. 12–14, the level of which has in many respects still not been surpassed today. These studies showed in particular that near the fission threshold in the region of lead the cross section is 10^{-33}–10^{-34} cm^2, a result that cannot be achieved without the highest purity of the targets used in the experiments; for the admixture of the many times more strongly fissioning actinides Th and U must not be greater than 10^{-8}%.

The possibilities for investigating low-energy fission of the preactinides are determined not only by the purity of the targets, though this is a very important condition, but also by the factors that characterize the entrance channel. Since the interaction of a charged particle (Z_i, A_i) with a nucleus (Z_t, A_t) is hindered by the Coulomb barrier

$$V^i_{\text{Coul}} \simeq \frac{Z_i Z_t}{A_i^{1/3} + A_t^{1/3}} \frac{e^2}{r_0}, \tag{17}$$

the reaction cross section, which is proportional to the barrier penetrability, decreases exponentially as particle energy $E_i < V^i_{\text{Coul}}$. As a result of this, only the region of excitation energies

$$E \geqslant V^i_{\text{Coul}} + Q_i,$$

where Q_i is the reaction energy, of the compound nucleus is favorable for investigations with a given particle. Table I gives the values of Q_i and V^i_{Coul} characterizing the reactions that lead to the formation of the nuclei ^{210}Po and ^{186}Os following bombardment of the corresponding target nuclei by various ions from ^{1}H to ^{12}C.

Figure 1 shows the dependence of the height of the fission barrier and the neutron binding energy on the mass number for the compound nuclei corresponding to the β-stability valley[15]:

$$A - 2Z = 0.4A^2/(A + 200). \tag{18}$$

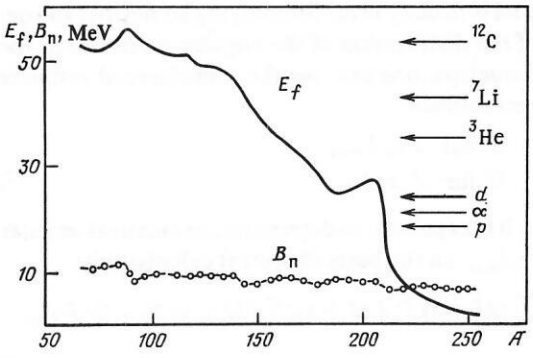

FIG. 1. Dependence of the height of the fission barrier E_f and the neutron binding energy B_n on the mass number A for nuclei near the valley of greatest β stability (18). The arrows indicate the excitation energies that bound below the regions of most favorable use of the various particles for studying fission of the preactinides (see the text).

It can be seen that in reactions with ^{3}He (we shall henceforth call ^{3}He ions τ ions) and heavy ions the region of the fission threshold for a large region of nuclei with $A > 150$ is effectively inaccessible. Therefore, near-threshold energies are mainly studied by protons and α particles, since in the (d, f) reaction there is an additional background due to disintegration of the deuteron in the Coulomb field of the nucleus and fission of impurities with high fissility by the produced neutrons.

In this review, we restrict ourselves to considering the fission cross sections of the preactinide nuclei in the region of excitation energies $E < 80$ MeV. This region is, on the one hand, effectively free of a contribution of fission after the direct nuclear interactions[16] and, on the other, emission fission does not yet become in it a source of significant error in the determination of the barrier height E_f of the initial state of the nucleus. To reduce the uncertainty in the results of the analysis, we shall also not discuss reactions with heavy ions with $A_i > 4$. It can be seen from the relation (9) that information about E_f is contained mainly in the width ratio Γ_f^0/Γ_n^0 for zero angular momentum. Allowance for the distribution of the angular momenta in the compound nucleus, which is characterized by the factor $\bar{\gamma}(J_{\max})$, merely complicates the main problem (the determination of E_f). In reactions with heavy ions, the influence of the angular momenta is very great, and all the errors in describing the factor $\bar{\gamma}(J_{\max})$ are in fact carried over into the uncertainty in the deduced barrier heights E_f.

Before we turn to the detailed discussion of the experimental data, we must establish more accurately the upper boundary of the region of the considered nuclei. In accordance with the periodic table, the first actinide is actinium, while radium is the heaviest preactinide. However, in many properties important for fission physics (shape of the potential barrier, equilibrium deformation, nucleon composition, and so forth), Ra is similar to the actinides. We recall that because of instability of the nuclei there are no targets between Ra and Bi suitable for investigating fission cross sections. We use this natural break in the sequence of stable elements and take the preactinide target nuclei as beginning with Bi. Such a division is also justified by the fact that any

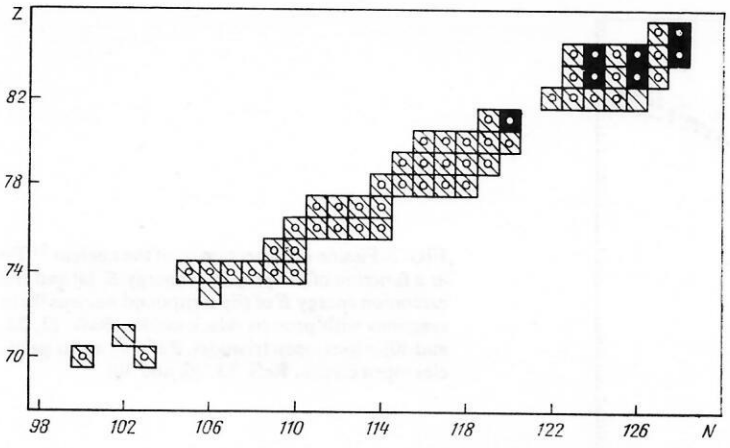

FIG. 2. Chart of the compound nuclei for which the fission probability has been studied experimentally as a function of the excitation energy in reactions with light ($A_i \leqslant 4$) charged particles. The black cells represent nuclei investigated as far as the fission threshold; the hatched shells, nuclei investigated in the above-threshold region of energies; the circle in the middle of a cell indicates nuclei investigated by the Alma-Ata cyclotron.[20–25]

reaction with absorption of a proton or a heavier charged particle by radium would lead to fission of an actinide nucleus.

Characteristic properties of the cross sections and angular anisotropy of the fission

Figure 2 is a chart of the fissioning nuclei for which the energy dependence of the fission cross section $\sigma_f(E_i)$ has been studied experimentally (Refs. 9–14 and 17–25). For many of the indicated nuclei, not only the integrated cross sections but also the angular anisotropy of the fission has been measured. More complete information about the studied reactions is given below, together with the results of the analysis of the experimental data. We here mention only that for the overwhelming majority of nuclei the fission cross sections have been measured in the essentially above-barrier region of energies. As will be shown below, experimental data on the parameters of the statistical description of the cross sections, including the barrier height E_f, are more informative, the wider the energy range of the investigated cross sections. For this reason, we shall not, as a rule, consider studies in which the measurements have been made for isolated energy values.

We discuss the most typical examples of the energy dependence of the fission cross sections and angular anisotropy observed in reactions with different charged particles. Figure 3 shows experimental data on the cross sections of the reactions ^{206}Pb(α, f), ^{207}Pb(τ, f), and ^{209}Bi(p, f), which lead to fission of the same compound nucleus ^{210}Po. In the left-hand part of the figure, the fission cross sections are represented as functions of the energy E_i of the incident particles. For α particles, the section of rapid growth of the cross sections is shifted relative to the cross sections of proton-induced fission, and the shift corresponds to the difference $\Delta Q = Q_p - Q_\alpha \simeq 10.4$ MeV between the reaction energies (see Table I). For protons and τ ions, the analogous difference has the opposite sign, $\Delta Q \simeq -3.5$ MeV, and in this case one would expect a corresponding shift of the fission cross sections in the opposite direction to that for the α particles. In the upper section of the considered region of energies of the incident particles, the expected shift of the cross sections is observed (Fig. 3a), but with decreasing energy of the particles it disappears. The reason for this effect is the influence of the Coulomb barrier.

For protons, the complete investigated range of energies E_p is situated well above V^p_{Coul} (see Table I). For τ ions, the Coulomb barrier is twice as large, and its influence leads to a decrease in the cross sections for production of a compound nucleus and the associated fission cross sections at particle energies, $E_\tau \lesssim 35$ MeV. The effect of the Coulomb barrier can be more clearly traced if for different particles the reaction cross sections are represented as functions of the

TABLE I. Reaction energy Q and height of the Coulomb barrier V_{Coul} for different particles.

Particle	Q, Mev		V^*_{Coul}, MeV	
	^{210}Po	^{186}Os	^{210}Po	^{186}Os
p	+5	+6,5	14,4	13,4
d	+10,3	+12,1	13,9	13,0
τ	+8,4	+11,5	26,7	24,9
α	−5,4	−2,8	26,3	24,5
^{7}Li	+5,1	+7,5	37,4	34,8
^{12}C	−14,0	−14,0	69,2	64,0

*It is assumed that $r_0 = 1.2$ F.

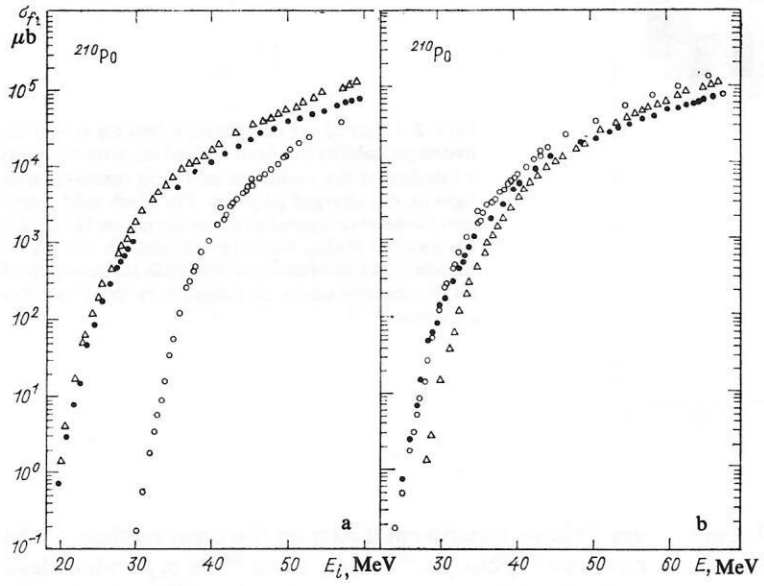

FIG. 3. Fission cross section σ_f of the nucleus ^{210}Po as a function of the projectile energy E_i (a) and the excitation energy E of the compound nucleus (b) in reactions with protons (black circles, Refs. 13, 22, and 30), τ ions (open triangles, Ref. 23), and α particles (open circles, Refs. 13, 20, and 30).

excitation energy of the compound nucleus (Fig. 3b). The cross sections of the (α, f) and (p, f) reactions, on which the Coulomb barrier has a very weak influence, are very similar in this representation, whereas the cross sections of the (τ, f) reaction deviate systematically with decreasing energy, and at the lower end of the considered energy range the discrepancy between them reaches almost two orders of magnitude.

Figure 4 gives data on the angular anisotropy of the fission of ^{210}Po in the same reactions for which the cross sections are given in Fig. 3.[13,22–25] The differences in the values and energy dependences of the angular anisotropy for the different particles can be understood qualitatively on the basis of the relation (16). In the first approximation, the observed angular anisotropy is determined by the ratio of the angular momentum introduced into the nucleus, $J^2_{max} = 2\langle J^2 \rangle$, and the parameter K_0^2, which depends solely on the excitation energy of the fissioning nucleus. For protons, the value of J^2_{max}, which is proportional to the product of the energy and the mass of the incident particle, is minimal, and to the (p, f) reaction there corresponds the least anisotropy (Fig. 4). At the same time, for α particles and τ ions the appreciable difference in the reaction energy $\Delta Q \simeq 14$ MeV (Table I) has the consequence that at the same excitation energies of the fissioning nuclei the τ ions have a much lower kinetic energy and accordingly introduce less angular momentum J^2_{max} into the nucleus. As a result, the anisotropy of the (τ, f) reaction differs little from that of the

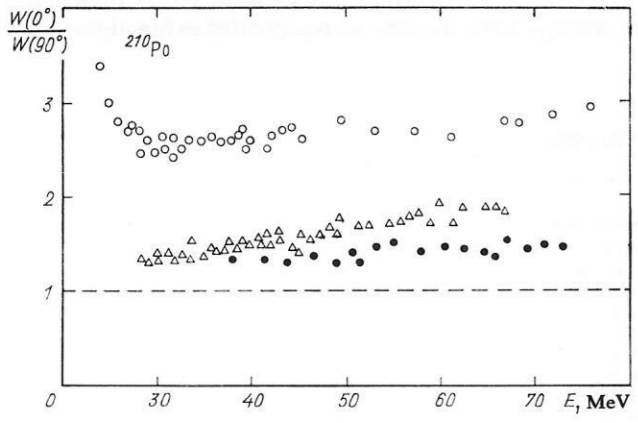

FIG. 4. Angular anisotropy $W(0°)/W(90°)$ of the fission as a function of the excitation energy E of the ^{210}Po nucleus in the reactions ^{209}Bi(p, f) (black circles, Ref. 30), ^{207}Pb(τ, f) (open triangles, Ref. 24), and ^{206}Pb (α, f) (open circles, Refs. 21, 30, and 51).

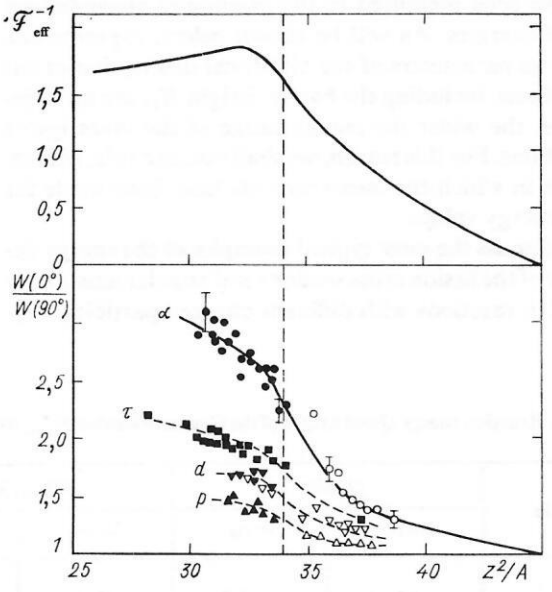

FIG. 5. Dependence on the parameter Z^2/A of the angular anisotropy $W(0°)/W(90°)$ of the fission (below) and of the reciprocal effective moment of inertia $\mathcal{F}^{-1}_{eff}$, expressed in units of the moment of inertia of the equally large sphere.[27] The experimental data are as follows: α particles with $E_\alpha = 42$ MeV (black circles, Ref. 21; open circles, Ref. 26); τ ions with $E_\tau = 60$ MeV (black squares, Ref. 24); deuterons with $E_d = 22$MeV (inverted black triangles, Ref. 25; inverted open triangles, Refs. 8 and 11); protons (black triangles, Ref. 22, $E_p = 28$ MeV; open triangles, Ref. 8, $E_p = 10$ MeV); the curves are drawn through the points.

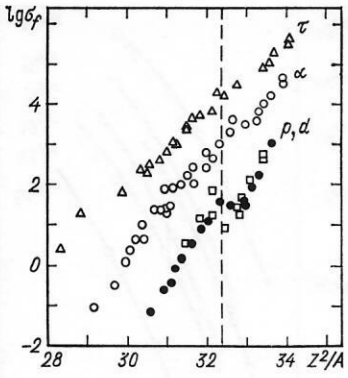

FIG. 6. Dependence of the logarithm of the fission cross section, $\log \sigma_f$ [μb] on the parameter Z^2/A. The experimental data correspond to the maximal energy of the particles in the Alma-Ata cyclotron. For τ: 60 MeV (Ref. 23); α: 50 MeV (Ref. 20); d: 25 MeV (Ref. 25); p: 30 MeV (Ref. 22). The vertical broken line corresponds to the nucleus ^{208}Pb.

(p,f) reaction despite the appreciable difference between the masses of the particles.

Figure 5 shows the angular anisotropy $W(0°)/W(90°)$ as a function of the parameter Z^2/A, which characterizes the fissility in the liquid-drop model.[1,15] Besides the data for the preactinides, Fig. 5 also gives the results of measurements of the anisotropy in the heavier actinide nuclei ($Z^2/A > 34$).[8,11,26] It can be seen from the relation (16) that the variations of the anisotropy at fixed energy of the incident particles reflect the changes in the parameter K_0^2. Since the parameter K_0^2 is determined above all by the effective moment of inertia $\mathscr{T}_{\text{eff}}$ of the fissioning nuclei, investigation of the fission anisotropy makes it possible to follow directly the dependence of $\mathscr{T}_{\text{eff}}$ on Z^2/A. The upper part of Fig. 5 gives the dependence on this parameter for the reciprocal effective moment of inertia $\mathscr{T}_{\text{eff}}^{-1}$, predicted by the liquid-drop model.[27] It can be seen that its main feature is a "bend" at $Z^2/A \simeq 33$–34, and this is clearly manifested in the observed behavior of the fission anisotropy.

Thus, the data given in Fig. 5 serve as a direct confirmation of the transition from ellipsoidal saddle configurations of the fissioning actinides to the dumbbell-shaped saddle configurations of the preactinide nuclei expected in accordance with the liquid-drop model. The experimental verification of this prediction was begun by the investigation of the fission of preactinide nuclei using the Alma-Ata cyclotron.[28]

Figure 6 shows the dependence on the parameter Z^2/A of the fission cross sections at fixed energy of the incident particles. The growth in the cross sections with increasing value of this parameter basically reflects the changes in the barrier heights shown in Fig. 1. However, it is noteworthy that for particles of high energies (τ and α) the dependence of $\log \sigma_f$ on the mass number is nearly linear. At the same time, for particles of lower energies (p and d) it can be seen that there are deviations from such a dependence in the neighborhood of ^{208}Pb (the broken line in Fig. 6), these reflecting the influence of shell effects is nearly magic nuclei. Below, we shall discuss in more detail the manifestation of these effects.

Properties of the entrance channel and transition from the cross sections to the fissility

It is seen from the discussion of Fig. 3 above that the properties of the entrance channel have a significant influence on the value and energy dependence of the fission cross sections. The transition from the fission cross sections (1) to the fissility (2) makes it possible to weaken this effect to the greatest extent.

In the analysis of the fissility it is assumed in the majority of studies that the cross section σ_c for production of a compound nucleus is equal to the reaction cross section σ_R predicted by the optical model. However, investigations made in recent years of nonequilibrium (noncompound) processes have shown that in the range of particle energies in which we are interested the differences between σ_c and σ_R may be fairly large. For the particles which we consider, the corresponding reaction cross sections are shown in Fig. 7. The points are the values of σ_R and the angular momentum $[J_{\max}^R]^2$ obtained by analysis of the differential cross sections of elastic scattering of particles.[29] The central part of Fig. 7 shows the cross sections $\sigma_c = \sigma_R - \sigma_{nc}$ determined by empirical analysis of the integrated contribution $\sigma_{nc}(E_i)$ of the nonequilibrium processes.[30]

The energy dependence $J_{\max}^2(E_i)$, which determines the maximal angular momentum of the compound nucleus in the semiclassical approximation, can be represented in the form

$$[J_{\max}^{(R)}]^2 = 2\langle J^2 \rangle_{\text{opt}} = C_1 E_i - C_2. \tag{19}$$

From approximation of the results of optical calculations of

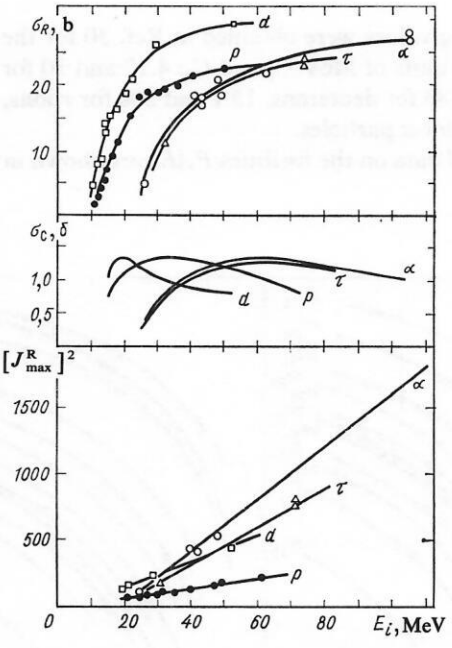

FIG. 7. Dependence of the reaction cross sections σ_R, the cross sections σ_c for formation of a compound nucleus, and the square of the maximal angular momentum of the reaction, $[J_{\max}^{(R)}]^2$, on the energy E_i of the particles.[30] The points show the reaction cross sections and the angular momenta obtained on the basis of the optical model.

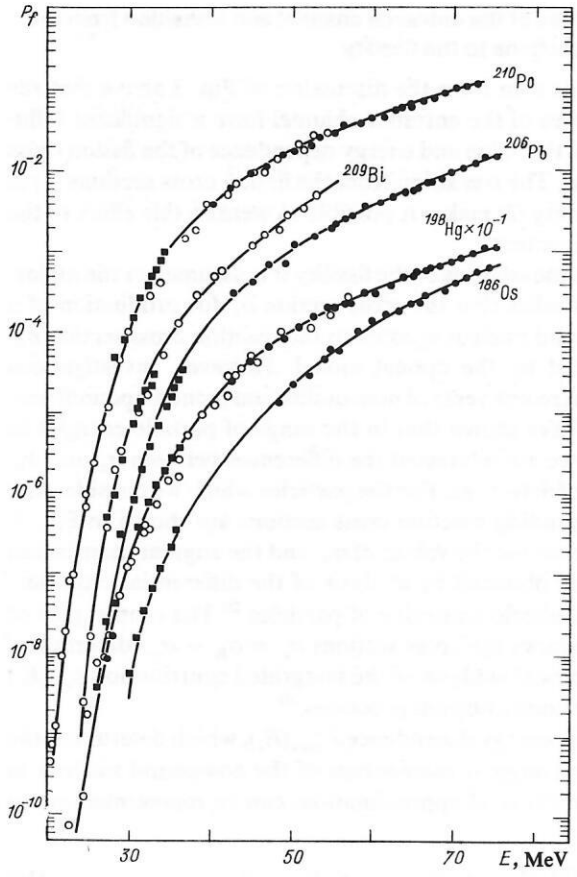

FIG. 8. Experimental data on the fissility $P_f(E)$ in the (p,f) reaction and their theoretical description[62]: black squares, Ref. 22; black circles, Ref. 30; open circles, Ref. 13.

$\langle J^2 \rangle$ the following values were obtained in Ref. 30 for the coefficients C_1 (in units of MeV^{-1}) and C_2: 4.17 and 30 for protons, 10.9 and 83 for deuterons, 15.1 and 286 for τ ions, and 20.3 and 398 for α particles.

Experimental data on the fissilities $P_f(E)$ are shown in

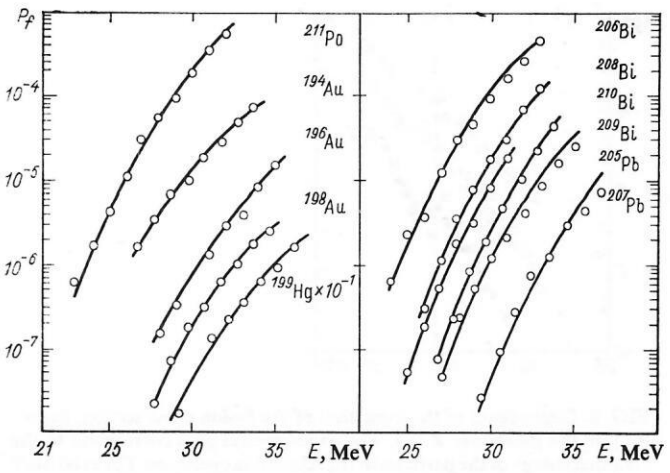

FIG. 9. Experimental data on the nuclear fissility $P_f(E)$ in the (d,f) reaction and their theoretical description[62]: open circles, Ref. 25.

Figs. 8–11. For the (d,f) and (τ,f) reactions, which have been investigated systematically only in Refs. 24 and 25, Figs. 9 and 10 give all the available experimental data. But for the (p,f) and (α,f) reactions, which have been investigated in many studies, we have restricted ourselves in Figs. 8 and 11 to the most characteristic nuclei, for which experimental data have been obained in a wide range of projectile energies. In all the figures, the continuous curves show the theoretical description of the observed fissilities discussed in the following sections of the review.

Dependence of the fissility on the angular momentum

It is of great interest to compare the fissilities of the same compound nuclei excited in different ways because of the possibility of obtaining information about the influence on the fission probability of the differences in the reaction entrance channels expressed by the two factors σ_c/σ_R and $\bar{\gamma}(J_{max})$. We consider first the part played by the latter. At small values of the angular momentum transferred to the

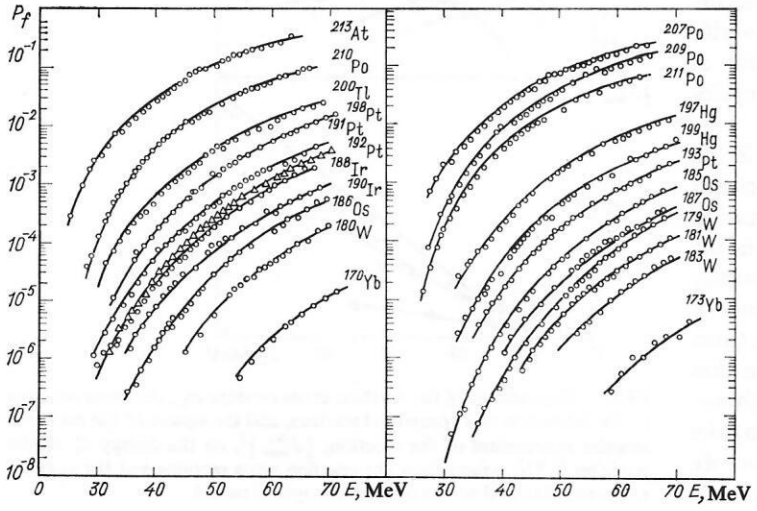

FIG. 10. Experimental data on the nuclear fissility $P_f(E)$ in the (τ,f) reaction and their theoretical description[62]: open circles and open triangles, Ref. 23.

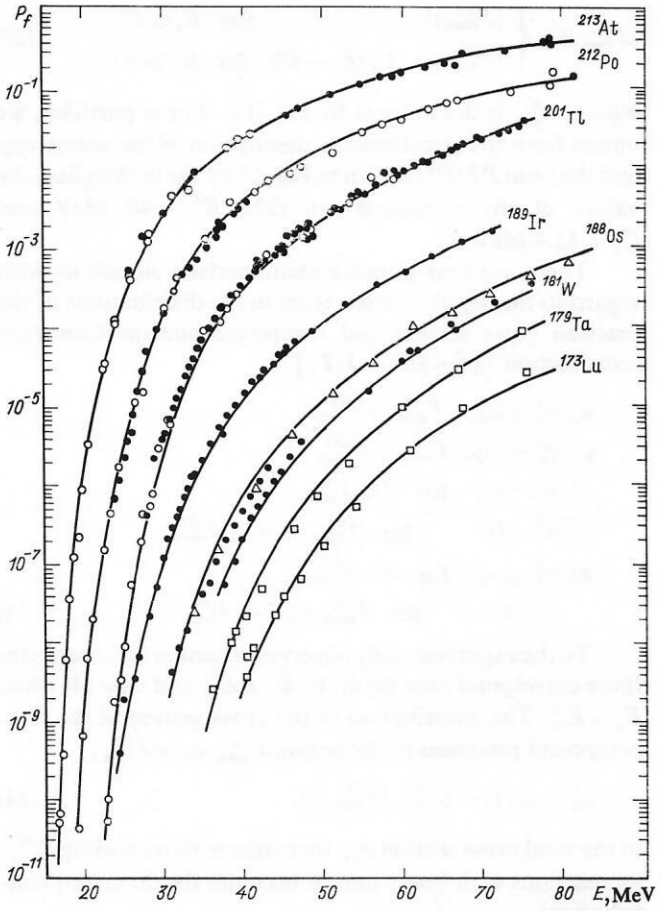

FIG. 11. Experimental data on the nuclear fissility $P_f(E)$ in the (α, f) reaction and their theoretical description[62]: black circles, Refs. 20 and 30; open circles, Ref. 13; open triangles, Ref. 14; open squares, Ref. 17.

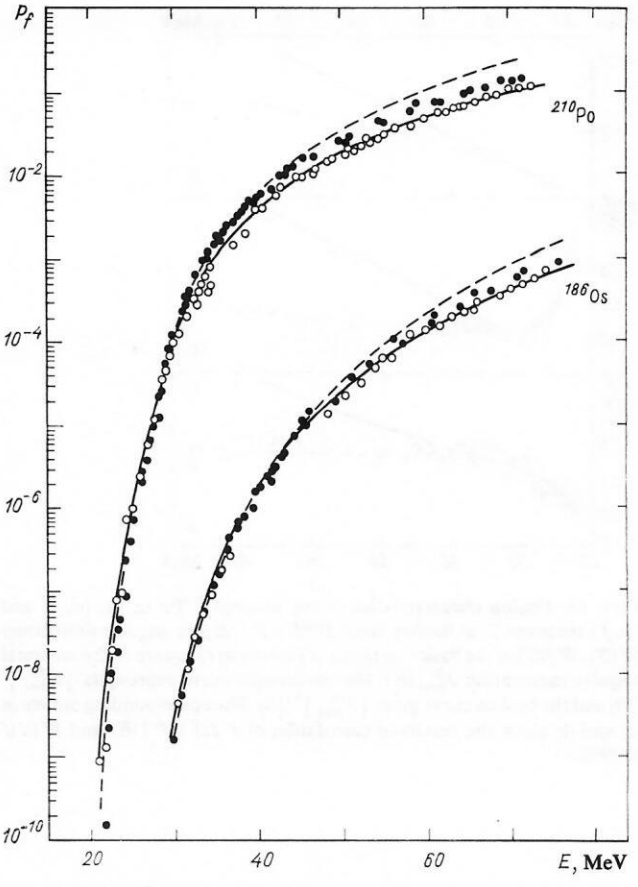

FIG. 12. Fissilities $P_f(E)$ of the nuclei ^{210}Po and ^{186}Os in reactions induced by α particles (black circles) and protons (open circles).[30] The curves represent calculations with $J_{max} = J^{(R)}_{max}$, the continuous curves for protons and the broken curves for α particles.

nucleus, the second factor can be represented in the form

$$\bar{\gamma}(J_{max}) \simeq 1 + \left(\beta K_0^2 - \frac{1}{6}\right)\frac{J_{max}^2}{2K_0^2} + \ldots \quad (20)$$

If $\beta K_0^2 > 1/6$, then $\bar{\gamma}(J_{max})$ increases with increasing angular momentum, and the fissility increases in proportion to it. Such influence of the angular momentum on the fissility is typical for excitation energies of the fissioning nuclei well above the barrier, and the corresponding effects have often been demonstrated in investigations with heavy ions.[3]

Figure 12 shows experimental data on the fissility of the nuclei ^{210}Po and ^{186}Os in reactions with protons and α particles.[30] In the region of high excitation energies, the α-particle fissility exceeds the proton fissility for the same nuclei, and this effect is a special case of the general tendency noted above. However, on the transition to lower energies both nuclei exhibit an "anomalous" dependence of the fissility on the mass of the particle, opposite to the traditional high-energy dependence. In Ref. 22, it was shown that a similar "anomalous" effect of the angular momentum transferred to the nucleus is observed systematically for all preactinide nuclei in which it has been possible to measure the cross sections of the (p, f) and (α, f) reactions sufficiently close to the fission threshold.

We note that when allowance was made for the differences between the cross sections $\sigma_c(E_i)$ and $\sigma_R(E_i)$ the proton and α-particle fissilities in the threshold region were found to agree better than in the previous determination of the fissilities in Ref. 22, but the anomalous growth of the fissility in the (p, f) reaction persisted.[30] The difference between the fissilities for the two reactions is best seen in Fig. 13a, which shows for the nucleus ^{210}Po the ratio $P_f^{\alpha}(E)/P_f^{p}(E)$. In the construction of this dependence $P_f^{p}(E)$ was represented by the calculated curve in Fig. 12, which passes effectively through the experimental points.

The nature of the anomalous influence of the angular momentum on the fissility can be readily understood by analyzing in the relation (20) the factor enclosed in the brackets. As the fission threshold is approached, this factor changes sign because of the decrease in $\sigma_{\perp f}$ and especially $\sigma_{\parallel f}$ [see (6)], and with increasing angular momentum the factor $\bar{\gamma}(J_{max})$ begins to decrease. A quantitative description of the fissility ratio

$$\frac{P_f^{\alpha}(E)}{P_f^{p}(E)} = \frac{\bar{\gamma}(J^{\alpha}_{max})}{\bar{\gamma}(J^{p}_{max})}, \quad (21)$$

made with the parametrization (19) of J_{max} given above, is

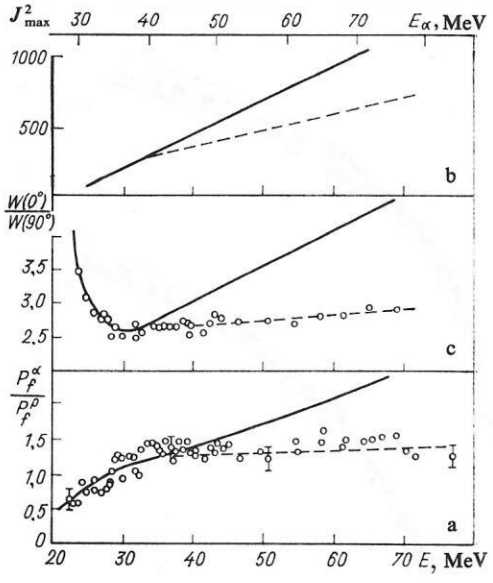

FIG. 13. Fission characteristics of the nucleus ^{210}Po in the (α,f) and (p,f) reactions[30]: a) fissility ratio $P_f^\alpha(E)/P_f^p(E)$; b) angular anisotropy $W(0°)/W(90°)$ of the fission in the (α,f) reaction; c) square of the maximal angular momentum $J^2_{max}(E)$: the continuous curve represents $[J^{(R)}_{max}]^2$ (19) and the broken curve gives $[J^{(c)}_{max}]^2$ (22). The corresponding curves in (a) and (b) show the results of calculation of $P_f^\alpha(E)/P_f^p(E)$ and $W(0°)/W(90°)$.

shown by the continuous curve in Fig. 13a. The allowance for this effect makes it possible to eliminate the disagreements in the determination of the threshold of the ^{206}Pb(α,f) and ^{209}Bi(p,f) reactions, which in the original analyses reached $\sim$1.0 MeV.[13,19]

Having achieved an explanation of the observed fissility ratio (21) in the threshold region, we nevertheless encounter the difficulty of simultaneous quantitative description of the fissilities of the two reactions at high excitations. A good description of the proton fissility can be obtained only at the price of discrepancies between the calculation and experiment that increase monotonically with the energy for the fissility in the (α,f) reaction. These discrepancies can be seen in Fig. 12, in which the continuous curve shows the results of calculations of $P_f^p(E)$ and the broken curve shows the results for $P_f^\alpha(E)$. Even more clearly are the discrepancies revealed in the ratio $P_f^\alpha(E)/P_f^p(E)$, shown in Fig. 13a. However, the discrepancy between the calculations and experiment can be eliminated if one assumes that beginning at certain energies $E_\alpha \gtrsim 40$ MeV compound nuclei are formed at lower angular momenta $J^{(c)}_{max}$ than predicted by the optical-model calculations (19). Such an assumption is also suggested by analysis of the angular anisotropy of the fission.[31]

The results of measurements of the fragment angular anisotropy $W(0°)/W(90°)$ in the ^{206}Pb(α,f) reaction are shown in Fig. 13b, from which it can be seen that the calculations deviate from experiment in the same energy region for the anisotropy and the fissility ratio. The discrepancies in both characteristics can be eliminated if one takes the energy dependence $J^{(c)}_{max}(E)$ in the form (Fig. 13c)

$$[J^{(c)}_{max}]^2 = \begin{cases} [J^{(R)}_{max}]^2 & \text{for } E_i \leqslant E_i^0; \\ [J^{(R)}_{max}]^2 - C_3(E_i - E_i^0) & \text{for } E_i > E_i^0, \end{cases} \quad (22)$$

where $J^{(R)}_{max}$ is determined by Eq. (19). For α particles, we obtain from the simultaneous description of the anisotropy and the ratio P_f^α/P_f^p, shown in Fig. 13 by the broken line, the values of the parameters in (22): $E_\alpha^0 = 40$ MeV and $C_3 = 12.4$ MeV^{-1}.

There are four possible characteristic situations with regard to the angular momentum in the distributions of the reaction cross section and compound-nucleus formation cross section $[\sigma_c^J \sim (2J+1)T_J]$:

a) $\sigma_c^J = \sigma_R^J$, $J^{(c)}_{max} = J^{(R)}_{max}$;
b) $\sigma_c^J < \sigma_R^J$, $J^{(c)}_{max} = J^{(R)}_{max}$;
c) $\sigma_c^J = \sigma_R^J$ for $J \leqslant J^{(c)}_{max}$,
$\sigma_c^J = 0$ for $J^c_{max} < J < J^{(R)}_{max}$;
d) $\sigma_c^J < \sigma_R^J$ for $J \leqslant J^{(c)}_{max}$,
$\sigma_c^J = 0$ for $J^{(c)}_{max} < J < J^{(R)}_{max}$. (23)

To the experimentally observed situation for α particles there correspond case (b) up to $E_\alpha < E_\alpha^0$ and case (d) when $E_\alpha > E_\alpha^0$. The contribution of the cross section of the non-compound processes in the region $J^{(c)}_{max} < J < J^{(R)}_{max}$,

$$\sigma'_{nc} = \sigma_R\{1 - [J^{(c)}_{max}/J^{(R)}_{max}]^2\}, \quad (24)$$

to the total cross section σ_{nc} increases with increasing $J^{(R)}_{max}$ (in reactions with heavy ions, it becomes the dominant contribution).

As is shown by analysis of the angular anisotropy of the fission fragments of the (p,f) reaction, there are also differences between $J^{(R)}_{max}$ and $J^{(c)}_{max}$ for protons.[32] The effect described by the relation (22) is evidently fairly general. However, in a discussion of the cross sections of the (p,f) and (d,f) reactions it can be ignored, since for both projectiles the deviation of the factor $\bar{\gamma}(J_{max})$ in the relation (9) from unity is negligible even for $J^{(c)}_{max} = J^{(R)}_{max}$. For the (τ,f) reaction, we adopted a dependence $J_{max}(E_\tau)$ similar to the one established for α particles with $E_\tau^0 = E_\alpha^0$ and $C_3 = 9.6$ MeV^{-1}.

3. FISSION PROBABILITY AND DENSITY OF NUCLEAR LEVELS

Shell effects in the density of neutron resonances and in the fissilities

To calculate the level density in the relations (3)–(5) of the statistical theory of nuclear reactions, it is very common to use the expressions of the Fermi-gas model[2,3]:

$$\rho(U, J) = \frac{2J+1}{24\sqrt{2}a^{1/4}(U-\delta)^{5/4}\sigma^3} \times \exp\left\{2\sqrt{a(U-\delta)} - \frac{(J+1/2)^2}{2\sigma^2}\right\}, \quad (25)$$

$$\sigma^2 = \frac{6\overline{m^2}}{\pi^2}\sqrt{a(U-\delta)}.$$

These expressions are fairly simple and contain only three parameters: the level-density parameter a, which is propor-

tional to the density of single-particle states near the Fermi energy, the mean square $\overline{m^2}$ of the projection of the single-particle angular momentum, and the correction δ for the even-odd differences in the nuclear level density. The correction δ is usually identified with the analogous correction to the mass formula, and the parameter $\overline{m^2}$ is chosen on the basis of a semiclassical estimate of the moment of inertia of the excited nuclei, $\overline{m^2} \simeq \pi^2 \mathscr{T}_0 / 6a \simeq 0.24 A^{2/3}$, and in this case the energy dependence of the nuclear level density is entirely determined by the parameter a.

At the present time, the most direct and reliable information about the level density of excited nuclei is obtained from experimental data on the density of neutron resonances. Analysis of these data by means of the relations (25) showed that the dependence of the parameter a on the mass number has deep dips in the region of nuclei with a magic number of nucleons, these indicating that shell effects in the excited nuclei play an important part.[33,34] To describe the dependence of the parameter a on the nucleon composition, one uses relations based on the correlation with the degeneracy of the subshells nearest the Fermi surface[33] or with the shell correction to the mass formula.[34] In both of these approaches, the parameter a is independent of the excitation energy, and as a consequence the shell effects persist in the level densities at arbitrarily high excitation energies.

More correct methods of calculating the nuclear level densities based on rigorous allowance for the discrete nature of the level spectrum of the shell model showed that the shell nonuniformities in the single-particle spectrum lead to a definite energy dependence of the parameter $a(U)$.[35] With increasing excitation energy, the shell effects in the level density become weaker, and at sufficiently high excitations the dependence of the parameter a on the mass number tends to the semiclassical value $\tilde{a} \simeq A/11$ MeV^{-1}. These important features in the behavior of the level-density parameter can be justified in a general form on the basis of the shell-correction method.[36,37]

Experimental data on the level-density parameter a extracted from analysis of the density of neutron resonances are shown in the upper part of Fig. 14. In the lower part, we give the experimental values of the shell corrections to the mass formula

$$\delta \mathscr{E}_0 = M_{\text{exp}}(Z, A) - \tilde{M}(Z, A, \varepsilon_0), \tag{26}$$

where M_{exp} is the experimental value of the mass defect, and $\tilde{M}$ is its liquid-drop component calculated for the equilibrium nuclear deformation ε_0.[15] The clear correlation between the shell correction and the observed variations of the parameter a reflect the intimate relationship between these quantities.

The correlation shown in Fig. 14 was used[38] to construct a phenomenological description of the level-density parameter $a(U)$ on the basis of the relation (25) of the Fermi-gas model. The connection between the parameter a and the shell correction $\delta \mathscr{E}_0$ was specified in the form

$$a(U, Z, A) = \tilde{a}(A)\left\{1 + \delta \mathscr{E}_0 (Z, A) \frac{f(U)}{U}\right\}, \tag{27}$$

where $\tilde{a}(A)$ corresponds to the asymptotic (liquid-drop) limit,

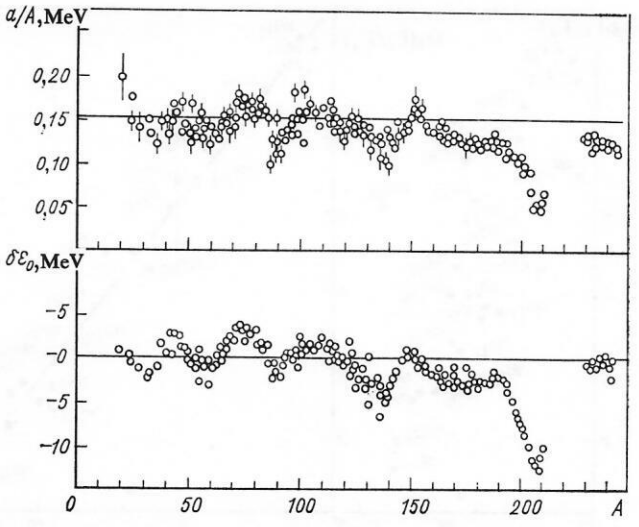

FIG. 14. Dependence of the level-density parameter $a(B_n)/A$ and the shell correction $\delta \mathscr{E}_0$ to the energy for equilibrium deformation of the nucleus on the mass number A.[38]

which is attained in practice at $U \sim 50$ MeV, while the dimensionless function $f(U)$ determines the behavior of $a(U)$ at lower energies. The form of the function

$$f(U) = 1 - \exp(-\gamma U), \tag{28}$$

which determines the rearrangement of the shells with varying energy, corresponds to the simplest approximation of the results of calculation of the thermodynamic functions of excited nuclei for a realistic level spectrum of the shell potential.[38] The parameters $\alpha = \tilde{a}/A \simeq 0.154$ MeV^{-1} and $\gamma = 0.054$ MeV^{-1} in (27) and (28) were found from the condition of best description of the experimental $a(B_n)$ data by the relation (27).

The effect of the rearrangement of the shells with the energy is manifested very clearly in the experimental values of the ratio Γ_f/Γ_n deduced from the fission cross sections of the preactinides. It was already noted in the early studies that at sufficiently high excitation energies $\gtrsim 50$ MeV the observed values of $\log(\Gamma_f/\Gamma_n)$ for a large number of nuclei can be approximated with good accuracy by a linear dependence on the liquid-drop model parameter Z^2/A.[39] With decreasing excitation energy, such a dependence is basically preserved, but the scatter of the experimental points increases appreciably. Since the points for nuclei in the region of the doubly magic nucleus ^{208}Pb are the ones that deviate most strongly from the general tendency, it is natural to associate these deviations with the manifestation of shell effects in the neutron channel.

The influence of the shell effects on the ratio Γ_f/Γ_n can be readily traced by means of the phenomenological parametrization of the level-density parameter considered above.[20] Apart from the pre-exponential factor, the relation (5) can be expressed in the form

$$\ln(\Gamma_f/\Gamma_n) \simeq 2\sqrt{a_f (E - E'_f)} - 2\sqrt{a_n (E - B'_n)} = \Delta S, \tag{29}$$

where E'_f and B'_n are the effective values of the fission bar-

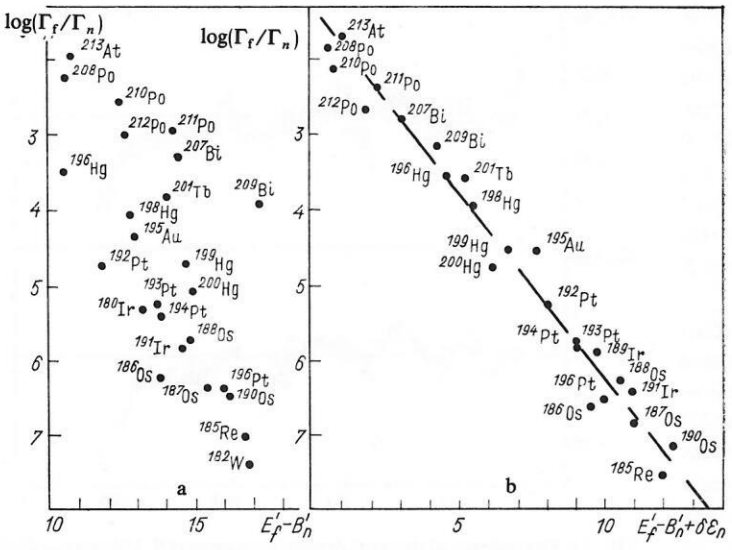

FIG. 15. Dependence of $\log(\Gamma_f/\Gamma_n)$ on the difference $E'_f - B'_n$ for $\tilde{U}_n = 30$ MeV and on $E'_f - B'_n + \delta\mathscr{E}_n$ for $\tilde{U}_n = 25$ MeV.[20]

rier and the neutron binding energy, both containing corrections for the even–odd differences of the level density; a_f and a_n are the level-density parameters for the fission and neutron channels. If to describe the energy dependence of the level-density parameter one uses the expression (27) and takes $\tilde{a}_f = \tilde{a}_n = \tilde{a}$, then the difference between the entropies of the fission and neutron channels will be determined by the relation

$$\Delta S = -\frac{E'_f - B'_n + f(U_n)\,\delta\mathscr{E}_n - f(U_f)\,\delta\mathscr{E}_f}{(\tilde{U}_n/\tilde{a})^{1/2}}, \qquad (30)$$

where $\delta\mathscr{E}_n$ and $\delta\mathscr{E}_f$ are, respectively, the shell corrections for the residual nucleus with equilibrium deformation and for the strongly deformed fissioning nucleus in the transitional state; $\tilde{a}$ is the asymptotic value of the level-density parameter at high excitation energy, and $\tilde{U}_n = E - B'_n + f(U_n)\delta\mathscr{E}_n$. If the shell dependence of the level-density parameter is ignored (i.e., one sets $\delta\mathscr{E}_n = \delta\mathscr{E}_f = 0$), then for fixed excitation energy in the neutron channel the ratio Γ_f/Γ_n must depend only on the difference $E'_f - B'_n$.

The variations in the observed values of Γ_f/Γ_n with the nucleon composition of the nucleus for given values of U_n and $\tilde{U}_n$ are shown in Fig. 15. The experimental data for $U_n = E - B'_n = 30$ MeV, shown in Fig. 15a, reproduce on the average the expected dependence on $E'_f - B'_n$, but the scatter of the points is very great, and they occupy almost the entire field of the figure. In Fig. 15b, the data on Γ_f/Γ_n are shown in their dependence on $E'_f - B'_n + \partial\mathscr{E}_n$ at fixed energy $\tilde{U}_n = 25$ MeV. It can be seen that allowance for the shell effects in the neutron channel leads to an alignment of the points in a nearly linear dependence. The value $\tilde{U}_n = 25$ MeV for the considered nuclei corresponds on the average to the energy $U_n = 30$ MeV, for which the data in Fig. 15a are shown.

The ordering of the chaotic picture (Fig. 15a) arises in Fig. 15b through the choice of the corresponding parameter on the abscissa and the fixing of the redetermined effective excitation energy. The abscissa in Fig. 15b differs somewhat from the numerator of the ratio (30), having a more complicated form, but this simplification is completely justified by the fact that in the neighborhood of the magic isotopes of lead $|\delta\mathscr{E}_n| \gg |\delta\mathscr{E}_f|$, and the value of the dimensionless function $f(U_n)$ is near unity. If E'_f and B'_n are expressed in terms of the analogous parameters $\tilde{E}'_f$ and $\tilde{B}'_n$ of the liquid-drop model,

$$\left.\begin{aligned} E'_f &= \tilde{E}'_f - \delta\mathscr{E}_0 + \delta\mathscr{E}_f, \\ B'_n &= \tilde{B}'_n - \delta\mathscr{E}_0 + \delta\mathscr{E}_n \end{aligned}\right\} \qquad (31)$$

and the explicit form of the function $f(U)$ is used, then ΔS can be expressed as

$$\Delta S = -\sqrt{\frac{\tilde{a}}{\tilde{a}}}\,\frac{\tilde{E}'_f - \tilde{B}'_n + \delta\mathscr{E}_f \exp(-\gamma U_f) - \delta\mathscr{E}_n \exp(-\gamma U_n)}{[E - \tilde{B}'_n + \delta\mathscr{E}_0 - \delta\mathscr{E}_n \exp(-\gamma U_n)]^{1/2}}. \qquad (32)$$

From this it can be seen that at sufficiently high excitations Γ_f/Γ_n is determined by the liquid-drop difference between the entropies of the fission and neutron channels, $\Delta\tilde{S} = -(\tilde{E}'_f - \tilde{B}'_n)/\tilde{t}$, i.e., it behaves as if the excitation energy was measured from the ground-state energy of the liquid-drop model.

Thus, the behavior of the ratio Γ_f/Γ_n observed for the preactinides is essentially a direct demonstration of the damping of the shell effects in excited nuclei.

Self-consistent allowance for shell, superfluid, and collective effects in the nuclear level densities

The description of the nuclear level density by the Fermi-gas model can be justified only at excitation energies that exceed the neutron binding energy. At lower energies, important parts are played in the nuclei by pairing correlations of the nucleons of superconducting type and by coherent collective effects, the influence of which does not reduce to any simple redefinition of the level-density parameter in the relations (25). A systematic and self-consistent description of all such effects can be obtained only on the basis of microscopic methods of simulation of the static properties of the excited nuclei.[40,41] Unfortunately, rigorous microscopic

methods of calculating the level density are very laborious, and this greatly restricts the possibilities of their practical application in the analysis of the experimental data. Therefore, it is important to develop a description of the level density that takes into account adequately the main ideas on the structure of highly excited nuclear states but is at the same time sufficiently simple and convenient for practical applications. Such a description was developed in Ref. 42.

When allowance is made for pairing correlations and coherent effects of a collective nature, the relation for the level density can be represented in the form

$$\rho\,(U,\ J) = \rho_{qp}\,(U,\ J)\,k_{vib}\quad (U)\,k_{rot}\ (U), \tag{33}$$

where ρ_{qp} is the density of quasiparticle (noncollectivized) excitations of the nucleus, and k_{vib} and k_{rot} are the coefficients of the increase in the level density due to the vibrational and rotational excitations, respectively.

In the adiabatic approximation,[37] the coefficient k_{rot} is determined by the shape of the nucleus:

$$k_{rot}^{adiab} = \begin{cases} 1 & \text{for spherical nuclei,} \\ \sigma_{\perp}^2 & \text{for deformed nuclei.} \end{cases} \tag{34}$$

This estimate is made under the assumption of mirror and axial symmetry of the shape of the deformed nuclei. The known stable nuclei in the region of the rare-earth elements $150 \leqslant A \leqslant 190$ and the actinides $A \geqslant 230$ have such a shape. This symmetry of the shape of the preactinides is evidently also preserved in the transitional states at the top of the barrier. For the nonaxial shapes that the fissioning actinide nuclei can have at the top of the barrier, the increase in the level density due to the rotational excitations becomes even greater.[37]

The coefficient of the increase in the density due to vibrational excitation of levels is determined in the framework of the microscopic approach[40,41] by the relation

$$k_{vib} = \prod_{\lambda} \left[\frac{1-\exp\left(-\omega_{\lambda}^{0}/t\right)}{1-\exp\left(-\omega_{\lambda}/t\right)}\right]^{g_{\lambda}}, \tag{35}$$

where ω_λ is the energy of the vibrational modes in the excited (heated) nucleus, ω_λ^0 are the energies of the quasiparticle excitations corresponding to these modes, and g_λ is the degeneracy of the collective modes. The presence of the energies of the quasiparticle excitations in (35) reflects the nonadiabatic nature of this increase in the level density. If the deviation of ω_λ from ω_λ^0 is small, the corresponding factor of the relation (35) tends to unity, and therefore the main contribution to k_{vib} is made exclusively by the coherent collective excitations with an appreciable difference $\omega_\lambda - \omega_\lambda^0$. It should be noted that in the framework of the microscopic approach the symmetry conditions of the nuclear Hamiltonian impose certain constraints on the vibrational and rotational excitations, and as a result of these the self-consistent microscopic calculations of k_{rot} may differ from the adiabatic estimate (34).

An estimate of k_{vib} can be readily found in the case of sufficiently heated nuclei by means of the formula obtained in the framework of the liquid-drop model,

$$k_{vib} = \exp\left\{1.694\left(\frac{\rho_0}{\hbar^2\alpha_0}\right)^{2/3} R_0^2 t^{4/3}\right\}, \tag{36}$$

where α_0 is the coefficient of surface tension, and ρ_0 is the nuclear matter density. If the value $\alpha_0 \simeq 1.2$ MeV/F^2 is substituted in (36), together with the mass formulas corresponding to the phenomenological parameters of the surface energy,[15] then for the level density in the region of the neutron resonances we obtain $k_{vib} \simeq 2$–4. This estimate may be somewhat too low, since the liquid-drop model for nonmagic nuclei gives energies of the vibrational excitations higher than the observed ones.

The influence of the pairing correlations of superconducting type on the nuclear properties can be characterized by the correlation function Δ_0, which directly determines the even–odd nuclear mass differences and the value of the gap $\sim 2\Delta_0$ in the spectrum of quasiparticle excitations of even–even nuclei. Also related to the correlation function is the critical temperature t_{cr} of the phase transition from the superconducting (superfluid) state to the normal state:

$$t_{cr} = 0.567\Delta_0. \tag{37}$$

To the critical temperature there corresponds the excitation energy

$$U_{cr} = 0.472 a_{cr}\Delta_0^2 - n\Delta_0, \tag{38}$$

where $n = 0$, 1, and 2 for even–even, odd, and odd–odd nuclei. Above the critical energy, the density of the excited states and the other thermodynamic functions of the nucleus can be described by the relations of the Fermi-gas model, in which it is necessary to use only the effective excitation energy

$$U^* = U - E_{cond}. \tag{39}$$

Here, E_{cond} is the condensation energy, which determines the lowering of the ground state of the system as a result of the correlation effects. In the approximation of a continuous spectrum, it is described by the relation

$$E_{cond} = 0.152 a_{cr}\Delta_0^2 - n\Delta_0. \tag{40}$$

When allowance is made for shell effects, the redefinition (39) of the energy must also be included in the phenomenological description of the energy dependence of the level-density parameter:

$$a\,(U,\ z,\ A) = \begin{cases} \tilde{a}\,(A)\left\{1 + \delta\ell_0\,(Z,\ A)\,\dfrac{f\,(U^*)}{U^*}\right\} & \text{for } U^* \geqslant U_{cr}; \\ a\,(U_{cr},\ Z,\ A) & \text{for } U^* < U_{cr}. \end{cases} \tag{41}$$

Below the phase-transition point (38), the relations for the thermodynamic functions of the nucleus have a complicated form, and we shall not discuss them. Relations convenient for practical calculations can be found in Refs. 42 and 43.

In the framework of the model described above, the number of parameters that characterize the excited nucleus remains practically the same as in the Fermi-gas model. In Ref. 42, this approach was used to analyze experimental data

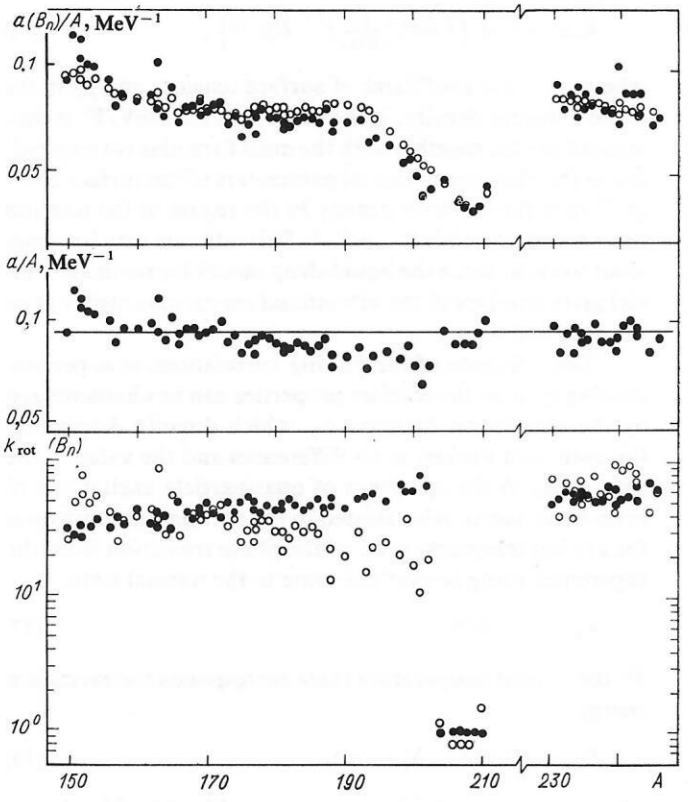

FIG. 16. Systematics of the level-density parameter $a(B_n)$ (at the top) and of the asymptotic values of this parameter $\tilde{a}$ (in the central part) obtained by analyzing the density of neutron resonances (black circles) and on the basis of the relations of the superfluid nuclear model (open circles).[42,57] The lower part of the figure shows the values of $k_{rot}(B_n)$ corresponding to the experimental values of $\tilde{a}/A$ (black circles) and to the values $\tilde{a}/A = 0.094$ MeV^{-1} (open circles).

on the density of the neutron resonances. The experimental values of the shell corrections,[15] shown in Fig. 15, were taken as $\delta\mathscr{E}_0$, and the correlation function of the nuclei was taken to be $\Delta_0 = 12/\sqrt{A}$ MeV. Minimization of the deviations of the calculated values of the level density from the experimental values determined the optimal value of the parameter $\gamma = 0.064$ MeV^{-1}. The level-density parameters $a(B_n)/A$ then obtained, and also the corresponding asymptotic values of the parameters $\tilde{a}/A$ are shown in Fig. 16.

For the regions of nuclei $150 \leqslant A \leqslant 190$ and $A \geqslant 230$, for which rotational sequences of low-lying levels are clearly expressed, and also for the spherical nuclei with $A \simeq 204$–210, which are close to the doubly magic lead isotope, the values found for the parameter $\tilde{a}$ are grouped near $\tilde{a}/A \simeq 0.094$ MeV^{-1}. However, in the region of transitional nuclei $190 \lesssim A \lesssim 200$ systematic deviations from the expected asymptotic values of $\tilde{a}$ appear. In order to demonstrate these deviations more strikingly, the lower part of Fig. 16 compares the adiabatic estimate of $k_{rot}(B_n)$ with the values of this parameter that would be required to obtain the observed density of neutron resonances under the assumption $\tilde{a}/A = 0.094$ MeV^{-1}. In the region of the transitional nuclei, the required values of the coefficient k_{rot} are 2–3 times less than the adiabatic estimate but appreciably above the liquid-drop estimate of the coefficients k_{vib} (37). Thus, for the transitional nuclei the description obtained for the level-density parameters must be used with a certain care.

At the first glance, it might seem that the constructed systematics of the level-density parameters does not differ strongly from that constructed for the density of neutron resonances on the basis of the relations of the Fermi-gas model (see Fig. 14). But this is not so—an important difference between the two cases is represented by the lower values of the level-density parameters obtained when allowance is made for collective effects. These values agree well both with the results of the theoretical calculations of the parameters a made for the level scheme of the Woods–Saxon potential[35] and with the experimental data extracted from the spectrum of inelastically scattered neutrons with energies up to 7 MeV.[44] Such agreement between the data appears very important, since the evaporation spectra are sensitive precisely to the value of the level-density parameter and not to the absolute level density. In the framework of the traditional Fermi-gas model, which does not take into account collective effects, it is impossible to explain the differences between the values of the parameter a deduced from the resonance data and the evaporation spectra.[44]

Intimately related to the results of the analysis of the density of the neutron resonances is the question of the difference between the asymptotic parameters of the level density in the fission and neutron channels; this question is very important for practical applications of the systematics of $a(U,Z,A)$ to the description of the nuclear fissilities.

The presence of a gradient in the distribution of the nucleon density in the nucleus leads to the appearance in the density of the single-particle states and the binding energy of components proportional to the nuclear surface. The value of these components is important for the correct description of processes associated with nuclear deformation. The surface component of the deformation energy can be deter-

TABLE II. Coefficient of the dependence of the asymptotic parameter of the level density on the mass number for different potentials (references are indicated by square brackets).

Single-particle potential	α, MeV^{-1}	β, MeV^{-1}	$\tilde{a}_f/\tilde{a}_n$	Reference
Rectangular well	0.073	−0.056	0.96	[45]
Oscillator	0.105	−0.091	0.95	[20]
Woods–Saxon potential	0.073	0.095	1.04	[35]
Self-consistent potential for Skyrme forces	0.055	0.063	1.04	[46]
Semiclassical estimate of the influence of the diffuse edge	0.069	0.215	1.10	[47]
Analysis of neutron resonances	0.073	0.115	1.05	[42]

mined fairly reliably on the basis of a semiempirical mass formula. Information on the surface component of the density of states is much more sparse. In the general case, the dependence of the asymptotic level-density parameter on the mass number can be represented in the form

$$\tilde{a} = \alpha A + \beta A^{2/3} B_s, \tag{42}$$

where B_s is the surface of the nucleus in units of the equally large sphere. In the relations given above for $\tilde{a}$, it was assumed that $\beta = 0$. Theoretical estimates of the coefficients α and β for different single-particle potentials are given in Table II. If in accordance with the estimate of the density of single-particle levels in a rectangular well we take the coefficient value $\alpha = 0.073$ MeV^{-1}, then from the description considered above for the experimental data with respect to the density of the neutron resonances (Fig. 16) we obtain $\beta = 0.115$ MeV^{-1}.[42]

An appreciable difference between the deformations of the nucleus in the equilibrium and transitional states must be manifested in the ratio $\tilde{a}_f/\tilde{a}_n$ of the asymptotic parameters of the level density in the fission and neutron channels systematically exceeding unity. For the saddle configurations of the preactinides, $B_s \simeq 2^{1/3}$. The ratio a_f/a_n corresponding to such an increase in the nuclear surface is shown in the last column of Table II. Note the fairly large differences between the coefficients α and β and also between the ratios $\tilde{a}_f/\tilde{a}_n$ for different shapes of the mean-field potentials. These differences are one of the reasons for the appreciable quantitative discrepancies between microscopic calculations of the level density made on the basis of the single-particle spectra of the modified oscillator potential of Nilsson and the Woods–Saxon potential.[35,48]

Influence of pairing correlations on the angular anisotropy of the low-energy fission of the preactinides

The characteristic feature in the behavior of the thermodynamic quantities in the superfluid nuclear model discussed above is the phase transition from the superfluid (superconducting) state to the normal Fermi-gas state. However, in a real nucleus, as opposed to superconductors, the concept of a phase transition is not rigorous, the number of particles being small.[49] Quantitatively, this feature of the nuclear system is manifested in a smoothing of the theoretical curves in the neighborhood of the critical point, their behavior to the left and right of it remaining essentially the same. For the neutron channel, the region of excitation energies below the critical value is not reflected in the fissility of the preactinides, since for them $E_f - B_n > U_{cr}$. But in the fission channel the section of excitation energies $U < U_{cr}$ has been studied fairly fully for a number of spherical nuclei in the neighborhood of lead. Nevertheless, even in these nuclei the phase transition in the entropy or in the parameter $a_f(U)$ cannot be readily followed, since in the energy dependence of the fissility they are played out on the background of the no less strong shell and collective effects.

It is a different matter with regard to the differential characteristic of the fissility represented by the angular anisotropy of the fragments. In the region of the preactinides, where $P_f(E) \ll 1$, the angular anisotropy of the fragments is, as was already noted in Sec. 1, effectively insensitive to the description of the ratio Γ_f^0/Γ_n^0, and, therefore to the simulation of the shell and collective effects in the neutron channel. From the analysis of the observed angular anisotropy one can determine by means of the relation (15) the quantity $K_0^2(U)$, and even better the effective moment of inertia $\mathcal{J}_{eff} = \mathcal{J}_\parallel (1 - \mathcal{J}_\parallel/\mathcal{J}_\perp)^{-1}$, which in the preactinides is, the inequality $\mathcal{J}_\parallel/\mathcal{J}_\perp \ll 1$ holding, close to the parallel moment of inertia. All these characteristics, particularly $\mathcal{J}_\parallel$, experience significant changes in the energy dependence on the transition through the critical point $U = U_{cr}$. The energy dependence of the parameter K_0^2 can be represented in the form of the relations[50]

$$\frac{K_0^2}{(K_0^2)_{cr}} = \begin{cases} U/U_{cr} & \text{for } U \leqslant U_{cr} \\ 1.21\,(U/U_{cr} - 0.32)^{1/2} & \text{for } U > U_{cr}, \end{cases} \tag{43}$$

which are conveniently parametrized for determining the critical values U_{cr} and $(K_0^2)_{cr}$ in the description of the experimental data.

The most detailed experimental data on the angular anisotropy of low-energy fission of the preactinides, to the discussion of which we restrict ourselves in the present paper, have been obtained for the isotopes $^{208,210-212}$Po in the (α, f) reaction.[21,51] They were analyzed on the basis of the relations (15) and (43) in Refs. 21, 50, and 52. The results of the most recent of these studies, Ref. 50, are given in Table III, which besides the adopted values of E_f and the values found for U_{cr} and $(K_0^2)_{cr}$ gives the values of t_{cr} and Δ_f calculated in

TABLE III. Results of analysis of the energy dependence of $K_0^2(U)$.

Fissioning nucleus	E_f, MeV	U_{cr}, MeV	$(K_0^2)_{cr}$	t_{cr}, MeV	Δ_f, MeV	Δ_f, Δ_0
^{212}Po	19.8	7.6	27.9	0.52	0.90	1.10
^{211}Po	20.5	8.1	30.2	0.56	0.99	1.20
^{210}Po	21.3	8.6	27.4	0.55	0.97	1.17
^{208}Po	20.2	8.6	29.2	0.55	0.97	1.18

accordance with the formulas given above. It is interesting to compare the value of Δ_f for the anomalously deformed transitional state of the nucleus with the analogous quantity $\Delta_0 = 12A^{-1/2}$ MeV for equilibrium nuclear deformations, and to this end the ratio Δ_f/Δ_0 is given in Table III.

The complete set of experimental data on the angular anisotropy is shown compactly in Fig. 17 in the form of the dimensionless dependence of $\mathcal{J}_{eff}/\mathcal{J}_{eff}^{cr}$ on t/t_{cr}. In its construction, the relations of the superfluid model and the parameters from Table III were used. The good agreement between the experimental data and the theoretical curve confirms the validity of the description of the statistical characteristics of the excited nuclei by the relations of the superfluid nuclear model. The values found for the correlation function Δ_f of the strongly deformed transition configurations only slightly exceed the correlation functions of the equilibrium states of the nuclei, this indicating a fairly weak dependence of the characteristics of the pairing interaction of superconducting type on the nuclear deformation. We note that in the past this question was a matter of doubt and was the subject of a prolonged discussion (Refs. 19, 21, and 50–56).

Differences between the fissilities of spherical and deformed nuclei

On the basis of the relation (34), which predicts a strong dependence of the coefficient of the rotational increase in the level density on the equilibrium deformation of the nucleus, one can draw very important qualitative conclusions about a significant difference in the behavior of the fissilities of spherical and deformed nuclei. The difference is almost entirely due to the magnitude and energy dependence of k_{rot}^n in the neutron channel. The fission of spherical nuclei ($k_{rot}^n = 1$) will, compared with deformed nuclei ($k_{rot}^n = \sigma_{\perp n}^2$), be characterized by a higher and more rapidly increasing fissility. In addition, this effect will be enhanced by the shell effects in the behavior of $\rho_{qp}^n(U)$ that arise from the smaller

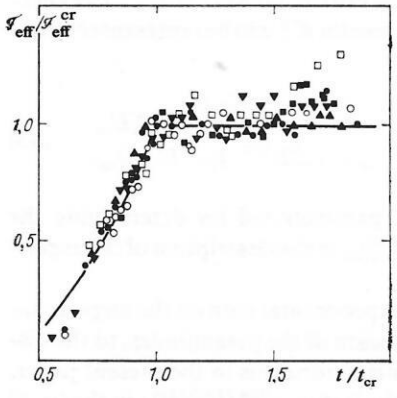

FIG. 17. Temperature dependence of the effective moments of inertia of the nuclei ^{208}Po (inverted black triangles), ^{210}Po (black and open circles), ^{211}Po (black and open squares), and ^{212}Po (black triangles).[50] The points are the results of analysis of the experimental data on the angular anisotropy of the fission (black symbols, Ref. 21; open symbols, Ref. 51). The curve represents the calculation in accordance with the superfluid nuclear model.

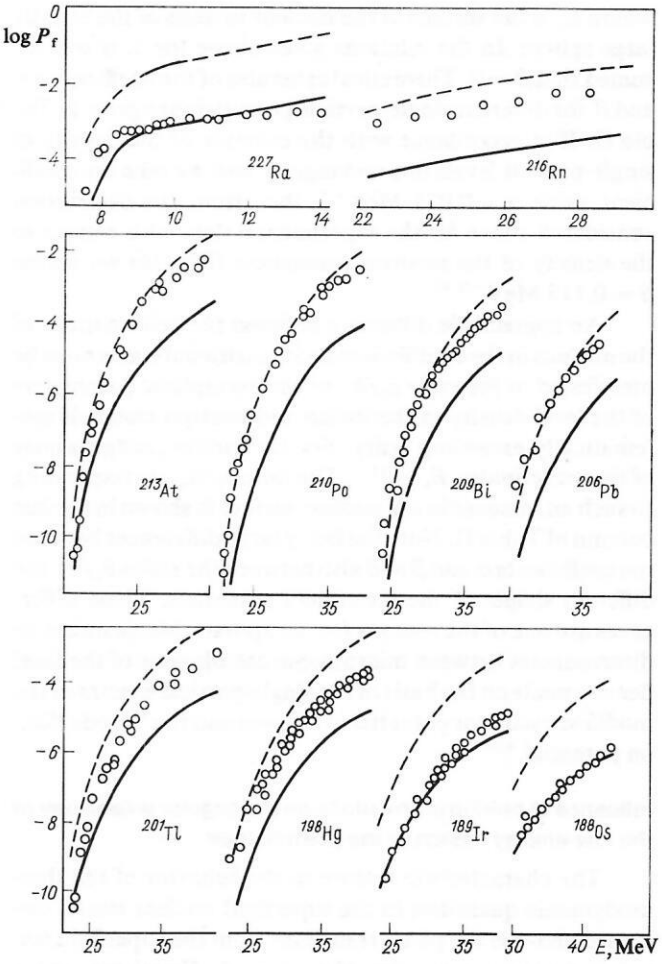

FIG. 18. Fissility $P_f(E)$ of some preactinides at excitation energies near the fission threshold: $E - E_f \lesssim 15$ MeV.[57] The open circles are the experimental values obtained in the following reactions: (α, f) for ^{213}At, ^{210}Po, ^{209}Bi, ^{201}Tl, ^{198}Hg, ^{189}Ir, ^{188}Os (Refs. 13, 14, and 20); (p, f) for ^{209}Bi, ^{206}Pb, ^{198}Hg (Refs. 13, 18, and 22); (n, f) for ^{227}Ra (Ref. 56) and $(^7$Li$, f)$ for ^{216}Rn.[58] The curves show the results of calculations, the broken ones for $k_{rot}^n = 1$ and the continuous ones for $k_{rot}^n = \sigma_{\perp n}^2$.

(than in deformed nuclei) values of the parameter $a_n(U)$ (see Fig. 16).

The difference between spherical and deformed nuclei that follows from this treatment is clearly manifested in the experimental data. Figure 18 shows the low-energy sections of the observed fissility of a number of preactinide nuclei ($E - E_f \lesssim 15$ MeV). For each of the nuclei, two calculated curves are given,[57] one of them corresponding to the assumption $k^n_{rot} = \sigma^2_{1n}$ (the lower), and the other to $k^n_{rot} = 1$. The fissilities $P_f(E)$ were calculated on the basis of the relations written down above with fission barriers E_f and shell corrections $\delta\mathscr{E}_n$ in the neutron channel of Myers and Swiatecki.[15] For the fission channel, $\delta\mathscr{E}_f = 0$, $\tilde{a}_f = \tilde{a}_n$, and $\Delta_f = 14/\sqrt{A}$ MeV were taken. This value of Δ_f follows from the results of the foregoing analysis of the energy dependence of the effective moments of inertia of the transitional configurations (Table III). The values of σ^2_{1f} and K^2_0 were calculated using the rigid-body moments of inertia of the fissioning nuclei found in the framework of the liquid-drop model with $(Z^2/A)_{cr} = 45$.[27] In the case of radium, we used the value $E_f = 8.3$ MeV (Ref. 56) and $k^f_{rot} = 2\sigma^2_{1f}$, in contrast to $k^f_{rot} = \sigma^2_{1f}$ for the remaining, lighter preactinides. The factor 2 takes into account the additional increase in the level density in the fission channel due to the pear-shaped asymmetry of the saddle configuration for the predominant asymmetric fission of ^{226}Ra(n,f).

In the analysis considered below, we did not take into account the difference between the coefficients k_{vib} in the fission and neutron channels. This simplifying assumption is justified by the fact that for deformed nuclei $k_{vib} \ll k_{rot}$ and $k^f_{vib}/k^n_{vib} \lesssim 2$ in accordance with the estimate (36). Therefore, on the background of the inaccuracies in the description of $k_{rot}(U)$ there is no point is separating the effect, small compared with them, associated with $k^f_{vib} \neq k^n_{vib}$.

Figure 18 is a clear demonstration of the influence of the collective effects on the level density $\rho_n(U)$, which is manifested in a shift of the experimental points from the upper curve for the spherical nuclei closest to the closed shell $Z = 82$, $N = 126$ (^{206}Pb,^{209}Bi,^{210}Po,^{213}At) to the lower curve on the transition to the deformed nuclei (^{188}Os,^{189}Ir,^{227}Ra) situated on either side of the region $A \simeq 208$. In its behavior, the nucleus ^{198}Hg corresponds to an intermediate case. Thus, the observed behavior of the fissility of the preactinides confirms the qualitative picture considered above of the expected manifestation of the collective effects in the level density and agrees overall with the classification of the nuclei adopted in the analysis of the density of the neutron resonances.

For several typical spherical and deformed nuclei the fissility $P_f(E)$ (experimental data and results of calculations) is shown in Fig. 19 in a wider range of energies. In the case of spherical nuclei, the fissility has been studied as far as the fission threshold, the position of which is determined by the section of most rapid decrease in $P_f(E)$ due to the decrease in the barrier penetrability in the subthreshold region. In such a situation, the determination of E_f depends weakly on the model used to describe the level density of the fission channel and, *a fortiori*, the neutron channel. This is a circumstance

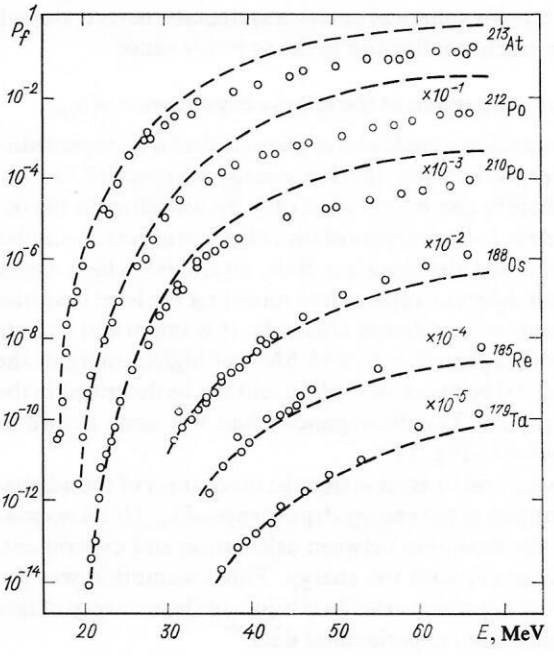

FIG. 19. Fissility of some spherical (^{213}At, ^{212}Po, ^{210}Po) and deformed (^{188}Os, ^{185}Re, ^{179}Ta) nuclei in a wide range of excitation energies.[57] The open circles represent the data of Refs. 2, 3, and 16, and the broken curves give the calculation of $P_f(E)$ for the values of k_{rot} corresponding to the adiabatic estimate.

very favorable for analysis, and it greatly reduces the uncertainty in the deduced parameters of the model. The calculated curves for the spherical nuclei in Fig. 19, fitted to the experimental data in the threshold region of energies, correspond to E_f values that differ from the Myers-Swiatecki barriers[15] by not more than 0.3 MeV.

It can be seen that when allowance is made for the coefficient $k^f_{rot} = \sigma^2_{1f}$ of the rotational increase in the level density in the fission channel the relations of the superfluid nuclear model give a fairly good description of the observed fissility up to an energy $\simeq 10$ MeV above the barrier, but at higher energies the calculated curve deviates upward from the experimental points for all the spherical nuclei. This effect was already seen in Fig. 18.

In the case of deformed nuclei, there are no factors such as shells in the ground state and the absence of rotational excitations which decrease the competing neutron channel and thus increase the fission probability of the spherical nuclei. Therefore, for the deformed nuclei in the immediate proximity of the threshold there are no experimental data on the fission cross section, which is evidently so small that it cannot be measured at the existing sensitivity of the methods. In this case, the determined value of E_f depends much more strongly on the model used in the statistical description of the experimental data. In Fig. 19, the calculated curves for the deformed nuclei are chosen in such a way that, under the assumption $k^f_{rot} = \sigma^2_{1f}$ and $k^n_{rot} = \sigma^2_{1n}$, a description of the section $P_f(E)$ at the lowest energies is obtained. It is noteworthy that the deviations of the calculated curves from the observed dependence then obtained for the deformed nu-

clei have, as for spherical nuclei, a systematic nature, though they are much smaller and in the opposite sense.

Empirical description of the energy dependence of k_{rot}

The analysis made above showed that a noncontradictory interpretation of the low-energy sections of the observed fissility can be achieved only by including in the description the level densities of the collective effects. A similar conclusion was also drawn in Refs. 59 and 60, which used a somewhat different approach to modeling the level densities of the neutron and fission channels. It is important to note that in the region $E - E_f \geqslant 15$ MeV of higher energies the experimental behavior of $P_f(E)$ could not be described in the quoted papers. The discrepancies had the same nature as those shown in Fig. 19.

It is natural to assume that the inaccuracy of the adiabatic description of the energy dependence of $k_{rot}(U)$ is responsible for the deviation between calculation and experiment, which increases with the energy. This assumption was the basis of the approach described below to the recovery of this dependence from experimental data.[57]

In the general case, a temperature dependence of the coefficient of the rotational increase in the level density convenient for practical calculations can be represented in the form

$$k_{rot}(t) = \begin{cases} 1 & \text{for spherical nuclei,} \\ k_{rot}^{adiab}(t)\, q(t) & \text{for deformed nuclei,} \end{cases} \tag{44}$$

where $q(t)$ is the function that characterizes the difference between $k_{rot}(t)$ and the adiabatic estimate. From the conditions of applicability of the adiabatic approximation there follows only an estimate of the behavior of $q(t)$ at comparatively low excitations of the nucleus: $q(t) \to 1$ as $t \to 0$. At the same time, because the collective and quasiparticle degrees of freedom are mixed in a highly excited nucleus, one must expect $k_{rot} \to 1$ as $t \to \infty$. In the region of intermediate excitation energies, we used the function $q(t)$ recovered directly from the experimental data, since theoretical information on the energy dependence of k_{rot} has as yet been obtained only for a highly simplified model.[61]

The function $q(t)$ can be found by analyzing the experimental fissility of spherical nuclei if one specifies the characteristics of the fission channel: the height of the fission barriers E_f, the shell correction of the nucleus $\delta\mathscr{E}_f$ in the transitional state, and the asymptotic value of the level-density parameter $\tilde{a}_f$.[57] For spherical nuclei in the neighborhood of lead, the fission cross sections have been measured to the threshold, the position of which is reliably fixed by the section of abrupt below-barrier decrease in the fissility, and this, as already noted, ensures a determination of E_f that is effectively independent of the level-density model. Also favorable for the analysis is the presence of experimental data for the chain of neighboring isotopes ^{210}Po, ^{211}Po, and ^{212}Po,[13,20] this making it possible to separate the fissility of the original nucleus, described by the relation (12), from the observed total fissility of the nuclei formed by cascade emission of neutrons. The same experimental information is available for the chain of isotopes ^{186}Os, ^{187}Os, ^{188}Os.[14,20] It

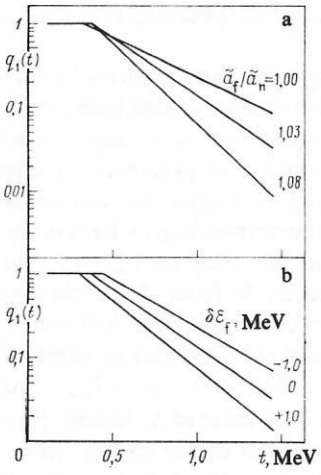

FIG. 20. Dependence of the function $q_1(t)$ under different assumptions about the parameters $\tilde{a}_f/\tilde{a}_n$ (a) and $\delta\mathscr{E}_f$ (b).[30]

is valuable for testing the consistency of the description of the spherical and deformed nuclei, the differences of which in the neutron channel are in accordance with (44) very appreciable.

In the analysis of the deviations of $k_{rot}(t)$ from the adiabatic estimate in the region of high energies it is more convenient to use in place of $q(t)$ the function

$$q_1(t) = \frac{k_{rot}(t) - 1}{k_{rot}^{adiab}(t) - 1} = \frac{q(t)\sigma_\perp^2(t) - 1}{\sigma_\perp^2(t) - 1}, \tag{45}$$

which at high temperatures ($t \to \infty$) has the asymptotic behavior $q_1(t) \to 0$. The temperature dependence of the function $q_1(t)$ was determined in Ref. 30 from the conditions of the best theoretical description of the observed fissility of the polonium isotopes under different assumptions about the magnitude of the shell correction $\delta\mathscr{E}_f$ and the ratios $\tilde{a}_f/\tilde{a}_n$. The results shown in Fig. 20a correspond to the assumption $\delta\mathscr{E}_f = 0$, which is usually made in the analysis of the fissility of preactinide nuclei. It is motivated by the small contribution of the shell component in the nuclear potential energy at large deformations in the transitional state near its limit—the scission configuration. If the accuracy of such an assumption is estimated at ± 1 MeV, then the values $\delta\mathscr{E}_f = \pm 1$ MeV lead to the variations of the function $q_1(t)$ shown in Fig. 20b. The relative difference between the curves increases with the temperature.

The considered variations of the parameters $\tilde{a}_f/\tilde{a}_n$ and $\delta\mathscr{E}_f$ affect only the value and the rate of change of the function $q_1(t)$, but they do not change its nature as a whole. To analyze the experimental data, the results of which are discussed in the following section, we used the function

$$q_1(t) = \begin{cases} 1 & \text{for } t \leqslant 0.354; \\ 3\exp(-3.1t) & \text{for } t > 0.354, \end{cases} \tag{46}$$

which is obtained in the description of the fissility of the nucleus ^{212}Po under the assumption that $\tilde{a}_f/\tilde{a}_n = 1.03$ and $\delta\mathscr{E}_f = 0$. The value $\tilde{a}_f/\tilde{a}_n = 1.03$ is obtained from the relation (42) for $\alpha = 0.073$ and $\beta = 0.115$ MeV^{-1}.

If the interpretation given above for the function $q(t)$ is

correct, it must be universal, i.e., its extension to other nuclei, and also to the neutron channel of deformed nuclei, must ensure description of the observed fissility in the complete range of energies.[57] We recall that without allowance for the established dependence of $q(t)$, i.e., for $k_{\rm rot}=\sigma_\perp^2$, there was a discrepancy between the calculation and experiment, this having opposite signs for spherical and deformed nuclei (see Fig. 19). This fact can be interpreted as a direct consequence of the decrease with the energy of the function $q(U)$, since in accordance with the definition of the latter we must have

$$\frac{P_f(A,\ E)}{P_f^{\rm adiab}\ (A,\ E)}=\begin{cases} q\,(E-E_f)<1 & \text{for spherical nuclei,}\\ \dfrac{q\,(E-E_f)}{q\,(E-B_n)}>1 & \text{for deformed nuclei,}\end{cases} \tag{47}$$

where $P_f(A,E)$ is the observed fissility of the nucleus A with excitation energy E, and $P_f^{\rm adiab}(A,E)$ is the same quantity calculated for the adiabatic estimate of $k_{\rm rot}(U)$. The assumption of "universality" of the function $q(t)$ is one of the main assumptions in the fissility analysis whose results are discussed in the present review.

Figure 21 gives examples of the description of the observed fissility and its first "chance" of fissility (the fissility of the original nucleus) for ^{211}Po,^{212}Po,^{187}Os,^{188}Os. For the second pair of nuclei, the ratio $\tilde a_f/\tilde a_n$ is 1.06–1.08, and in this connection we emphasize that the attempts to keep the value of $\tilde a_f/\tilde a_n$ used in the description of the ^{211}Po and ^{212}Po fissilities lead to appreciable discrepancies with experiment that cannot be eliminated by the choice of E_f. The increase in $\tilde a_f/\tilde a_n$ on the transition from Po to Os is evidently due to the increase in the nuclear surface in the transitional configurations of the lighter preactinides, and, as will be shown below, the chosen dependence is qualitatively confirmed by the results of the analysis of the fissility of the complete set of nuclei.

It was shown above that the uncertainties in our knowledge about the parameters $\tilde a_f/\tilde a_n$ and $\delta\mathscr{E}_f$ strongly affect the behavior of the function $q(t)$, primarily the rate of decrease with increasing t. For the main purposes of the analysis, it is important to know how these changes affect the final results, namely, the values determined for E_f and the description of the fissility. The results of an investigation of the uncertainty in E_f associated with the assumptions made about $\delta\mathscr{E}_f$ and $\tilde a_f/\tilde a_n$ in the determination of the function $q(t)$ are given in Table IV. It can be concluded from them that variations of

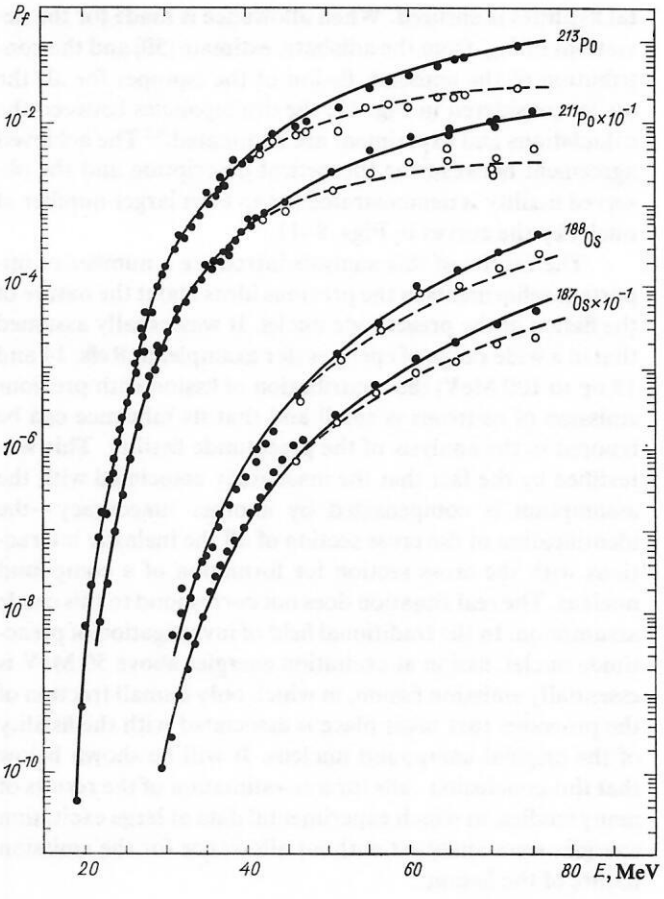

FIG. 21. Description of the fissility of the nuclei ^{211}Po, ^{212}Po, ^{187}Os, ^{188}Os.[30] The black circles show the observed fissility $P_f^{\rm obs}(A,E)$; the open circles, the fissility $P_f(A,E)$ of the original nuclei (first "chance") recovered in accordance with (12); the continuous curves, the results of calculation of the total fissility; and the broken curve, the results of calculation of the first-chance fissility.

the parameters have a rather weak effect on the determined values of E_f and $\tilde a_f/\tilde a_n$, namely:

a) a change in $\delta\mathscr{E}_f$ by $\pm$ 1 MeV for the spherical nuclei leads in the region of Os to a change in E_f by 0.2–0.3 MeV and in $\tilde a_f/\tilde a_n$ by 0.01–0.02 of the same sign;

b) an increase in $\tilde a_f/\tilde a_n$ for Po from 1.03 to 1.08 increases in the case of Os the values of E_f and $\tilde a_f/\tilde a_n$ by 0.5 MeV and 0.3, respectively.

We note that for all the characteristics in Table IV and in Fig. 20 practically the same description of the experimen-

TABLE IV. Influence of the parameters of ^{212}Po in the determination of the function $q(t)$ on the results of the analysis of the fissility of the deformed nuclei ^{187}Os and ^{188}Os.

^{212}Po			^{188}Os		^{187}Os	
$\delta\mathscr{E}_f$, MeV	$\tilde a_f/\tilde a_n$	E_f, MeV	$\tilde a_f/\tilde a_n$	E_f, MeV	$\tilde a_f/\tilde a_n$	E_f, MeV
+1	1,03	19,6	1,07	24,6	1,09	25,0
−1	1,03	19,6	1,04	24,1	1,07	24,6
0	1,00	19,6	1,04	23,9	1,06	24,3
0	1,03	19,6	1,06	24,4	1,08	24,8
0	1,08	19,6	1,09	24,9	1,11	25,3

tal fissilities is ensured. When allowance is made for the deviations of k_{rot} from the adiabatic estimate (50) and the contribution of the emission fission of the isotopes for all the nuclei considered in Fig. 19, the discrepancies between the calculations and experiment are eliminated.[62] The achieved agreement between the theoretical description and the observed fissility is demonstrated for an even larger number of nuclei by the curves in Figs. 8–11.

The results of this analysis introduce a number of important refinements in the previous ideas about the nature of the fission of the preactinide nuclei. It was usually assumed that in a wide range of energies (for example, in Refs. 14 and 19 up to 100 MeV) the contribution of fission with previous emission of neutrons is small and that its influence can be ignored in the analysis of the preactinide fissility. This was justified by the fact that the inaccuracy associated with the assumption is compensated by another inaccuracy—the identification of the cross section of all the inelastic interactions with the cross section for formation of a compound nucleus. The real situation does not correspond to this crude assumption. In the traditional field of investigation of preactinide nuclei, fission at excitation energies above 50 MeV is essentially emission fission, in which only a small fraction of the processes that takes place is associated with the fissility of the original compound nucleus. It will be shown below that this conclusion calls for a re-estimation of the results of many studies, in which experimental data at large excitation energies were analyzed without allowance for the emission nature of the fission.

4. RESULTS OF ANALYSIS OF FISSILITY

Electrofission of lead and bismuth

Before we turn to the presentation of the results of the fissility analysis, we consider one further group of experimental data—the probability of fission of the Pb and Bi isotopes by electrons with energy $E_e \lesssim 50$ MeV.[63–66] The analysis of this experimental information is interesting from two points of view. First, with the Pb isotopes there are associated a local maximum in the barrier heights $E_f(Z, A)$ (see Fig. 1) and, correspondingly, the deepest dip in the chart of the shell corrections in the binding energies of the nuclear ground states. We emphasize that electroexcitation is the only method of forming compound nuclei that has been used for the experimental study of ^{208}Pb and ^{207}Pb fission. Second, for two other nuclei, ^{209}Bi and ^{206}Pb, there are experimental data on the fissility in a wide range of proton energies, and these make it possible to test the consistency of the theoretical description of the fission probability for these strongly differing excitation methods.

In the (e, f) reaction, a broad distribution of the initial excitation energies is realized, this corresponding to the spectrum $N(E, E_e)/E$ of the virtual photons transferred by the electrons in the interaction with the nucleus. Therefore, an experiment measures directly, not the photofission cross section $\sigma_{\gamma f}(E)$, but the integrated yield

$$Y(E_e) = \int_0^{E_e} \frac{N(E, E_e)}{E} \sigma_{\gamma f}(E)\, dE = \int_0^{E_e} \frac{N(E, E_e)}{E} \sigma_{\gamma}(E)\, P_f(E)\, dE, \quad (48)$$

the analysis of which requires not only the photoabsorption cross section $\sigma_\gamma(E)$ but also knowledge of the virtual photon spectrum $N(E, E_e)$.

Figure 22 shows experimental data on the yields in the region $E_e \lesssim 50$ MeV,[63–66] which is fairly close to the fission threshold of the investigated nuclei. To describe the properties of the entrance channel of the (e, f) reaction, the assumptions of Ref. 64 were used, namely:

a) the virtual-photon spectrum was calculated in the DWBA;

b) as the photoabsorption cross section $\sigma_\gamma(E)$, the total cross section of the (γ, xn) processes for the ^{203}Tl nucleus measured in Ref. 67 was taken.

For the nuclei ^{209}Bi and ^{206}Pb, the theoretical $Y(E)$ curves in Fig. 22 were calculated with the parameters $E_f = 24.3$ and 25.3 MeV, respectively, and $\tilde{a}_f/\tilde{a}_n = 1.02$, these giving the best description of the fissilities of the same nuclei in the reactions ^{208}Pb(p, f), ^{207}Pb(d, f), ^{205}Tl(α, f) for

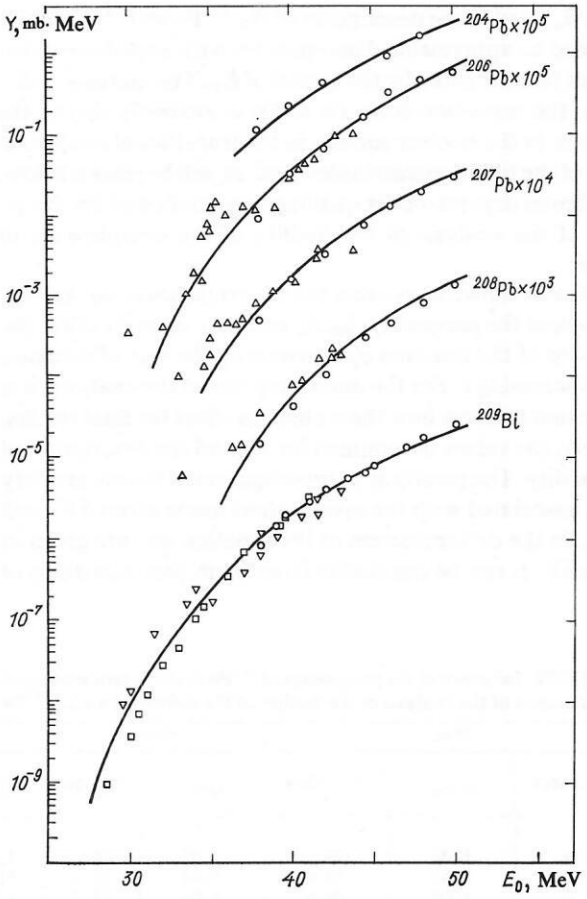

FIG. 22. Experimental data on the yields $Y(E_e)$ for the (e, f) reaction and their theoretical description[62]: open squares, Ref. 63; open circles, Ref. 64; open inverted triangles, Ref. 65; open triangles, Ref. 66.

TABLE V. Results of analysis of the fissility[62] and of the phenomenological description in the liquid-drop model[15] and in the droplet model[73] (references are indicated by square brackets).

Compound nucleus	Projectile particle and references	Energy range ΔE, MeV	Results of analysis of the fissility		Phenomenological description of E_f, MeV	
			$\tilde{a}_f/\tilde{a}_n$	E_f, MeV	[15]	[73]
^{213}At	α [13, 20, 30]	19—80	1,03	17,3	17,1	17,2
^{212}At	τ [23]	25—65	1,05	18,6	18,1	18,6
^{212}Po	α [13, 20, 30]	19—80	1,03	19,6	19,6	19,2
^{211}Po	α [13, 20]	22—80	1,035	20,6	20,5	20,5
	τ [23]	25—65	1,03	20,6		
	d [25]	15—25	1,03	20,5		
^{210}Po	α [13, 20, 30]	21—80	1,02	21,2	21,6	21,7
	τ [23]	28—65	1,02	21,2		
	p [13, 22, 30]	21—75	1,02	21,2		
^{209}Po	τ [23]	28—65	1,04	21,1	21,1	21,7
^{208}Po	α [20]	20—45	1,04	19,9	19,9	20,7
^{207}Po	τ [23]	25—65	1,04	19,3	19,0	20,1
^{210}Bi	d [25]	18—25	1,02	23,6	23,2	23,0
^{209}Bi	α [20]	25—45	1,02	24,3	24,3	24,2
	d [25]	18—25	1,02	24,4		
	p [13, 22, 30]	24—75	1,02	24,3		
	e [63, 64, 65]	28—50	1,02	24,2		
^{208}Bi	d [25]	18—25	1,04	23,6	23,8	24,0
	p [22]	26—35	1,02	24,1		
^{207}Bi	α [20]	25—45	1,04	22,9	22,6	23,0
	p [13, 22, 30]	25—55	1,03	22,8		
^{206}Bi	d [25]	16—25	1,03	22,4	21,8	25,3
^{208}Pb	e [64, 66]	33—50	1,02	27,4	27,3	26,6
^{207}Pb	d [25]	18—25	1,00	26,9	26,7	26,4
	e [64, 66]	33—50	1,02	27,0		
^{206}Pb	p [22, 30]	26—75	1,025	25,3	25,3	25,3
	e [64, 66]	30—50	1,02	25,3		
^{205}Pb	d [25]	16—25	1,00	24,6	24,2	24,7
^{204}Pb	p [22]	26—35	1,00	23,8	23,1	23,8
	e [64]	38—50	1,02	23,2		
^{201}Tl	α [13, 20, 30]	23—80	1.055	23,1	22,5	23,7
^{200}Tl	τ [23]	30—70	1,06	22,8	21,6	23,1
^{200}Hg	α [20]	25—47	1,02—1,05	24,6—23,5	24,0	24,8
^{199}Hg	α [20]	25—47	1,03—1,06	24,4—23,2	23,1	24,3
	τ [23]	30—70	1,05—1,06	24,7—23,4		
	d [25]	18—25	1,03—1,06	24,4—23,1		
^{198}Hg	α [20]	25—47	1,06—1,08	22,6—21,4	22,1	23,6
	τ [23]	30—70	1,06—1,08	22,7—21,4		
	p [9, 13, 22, 30]	25—75	1,06—1,07	22,7—21,6		
^{197}Hg	τ [23]	30—70	1,07—1,08	22,7—21,1	21,3	23,4
^{196}Hg	α [20]	25—47	1,06—1,09	21,2—19,7	20,2	22,4
^{198}Au	d [25]	18—25	1,02—1,05	24,9—23,7	24,3	25,0
^{197}Au	α [20]	40—48	1,04—1,06	25,1—23,6	23,2	24,3
	p [22]	32—36	1,05—1,06	24,8—23,4		
^{196}Au	d [25]	18—25	1,06—1,09	23,7—22,5	22,3	23,8
	p [22]	32—36	1,03—1,05	23,9—22,5		
^{195}Au	α [20]	40—47	1,05—1,06	22,7—20,8	21,5	23,2
	p [22]	29—35	1,03—1,04	22,9—21,3		
^{194}Au	d [25]	18—25	1,08—1,10	21,7—20,1	20,4	22,6
^{196}Pt	α [20]	25—47	1,06—1,08	26,3—24,9	24,9	25,0
^{194}Pt	α [20]	30—47	1,06—1,08	24,4—22,8	23,3	24,2
^{193}Pt	α [20]	30—47	1,08—1,10	24,2—22,7	22,1	23,5
	τ [23]	30—70	1,09—1,10	24,2—22,7		
^{192}Pt	α [20]	30—47	1,06—1,09	22,9—21,4	21,6	23,4
	τ [23]	30—70	1,07—1,09	23,1—21,5		
^{191}Pt	τ [23]	30—70	1,08—1,09	22,5—20,8	20,5	22,7
^{191}Ir	α [20]	30—47	1,12	23,2	22,8	24,5
	p [22]	30—35	1,11	23,2		
^{190}Ir	τ [23]	30—70	1,08	22,6	22,0	24,1
	p [22]	30—35	1,06	22,9		
^{189}Ir	α [20, 30]	25—76	1,08	22,0	21,4	24,1
	p [22]	31—35	1,08	22,1		
^{188}Ir	τ [23]	30—70	1,09	22,2	20,9	23,5
^{190}Os	α [20]	40—48	1,08	25,6	24,7	25,8
^{188}Os	α [14, 20]	30—80	1,06	24,4	23,8	25,6
^{187}Os	α [14, 20]	30—80	1,08	24,8	23,1	25,4
	τ [23]	35—70	1,08	24,6		
^{186}Os	α [14, 20, 30]	30—80	1,08	24,1	22,8	25,3
	τ [23]	35—70	1,08	24,1		
	p [22, 30]	30—75	1,08	24,1		
^{185}Os	τ [23]	35—70	1,09	24,0	22,1	25,1
^{185}Re	α [8, 20]	40—80	1,10	26,2	24,6	26,7
^{184}Re	p [22]	32—36	1,08	26,3	24,3	26,7
^{184}W	α [20]	40—48	1,09	27,4	26,4	28,0
^{183}W	τ [23]	50—70	1,08	28,3	26,3	28,3
^{182}W	α [20]	40—48	1,09	27,4	25,8	28,1
^{181}W	α [20, 30]	37—75	1,085	26,9	25,2	28,0
	τ [23]	40—70	1,08	27,0		

Continuation of Table V.

Compound nucleus	Projectile particle and references	Energy range ΔE, MeV	Results of analysis of the fissility		Phenomenological description of E_f, MeV	
			$\tilde{a}_f/\tilde{a}_n$	E_f, MeV	[15]	[73]
^{180}W	α [20]	40—48	1.10	26.6	24.7	27.7
	τ [23]	45—70	1.09	26.5		
^{179}W	τ [23]	35—70	1.09	25.8	24.3	27.6
^{179}Ta	α [19]	35—75	1.08	28.6	26.7	29.0
^{178}Lu	α [19]	35—75	1.07	30.5	29.0	31.7
^{178}Yb	τ [23]	55—70	1.08	33.4	31.6	33.7
^{170}Yb	τ [23]	55—79	1.08	30.6	29.9	32.9

bismuth and the reaction ^{205}Tl(p,f) for lead. Bearing in mind a certain discrepancy between the experimental data of the Darmstadt[63,64] and Toronto[65,66] groups, it is difficult to obtain a description better than that achieved with these parameters.[62]

Fission barriers and asymptotic level-density parameters

The results of the analysis of the complete set of experimental data on the fissility of preactinide nuclei[62] that we considered are given in Table V. The fourth and fifth columns give the parameters $\tilde{a}_f/\tilde{a}_n$ and E_f obtained by fitting to the experimental data. For the region of the transitional nuclei Hg–Pt, the analysis was made with the two assumptions $k^n_{\rm rot} = \sigma^2_{\perp n} q(t)$ and $k^n_{\rm rot} = 1$, and therefore Table V gives values of both parameters corresponding to each of these assumptions (the larger values of E_f correspond to the case $k^n_{\rm rot} = 1$).

The experimental fissility data are very diverse in different ranges of investigated energies and depending on their proximity to the fission threshold. This circumstance greatly influences the errors in the results of the analysis. In particular, the narrower the studied energy range, the wider the set of parameters E_f and $\tilde{a}_f/\tilde{a}_n$ by means of which approximately the same description of the experiment is ensured. Depending on the energy, the sensitivity of the fissility to the parameters E_f and $\tilde{a}_f/\tilde{a}_n$ is different—as the threshold is approached, the accuracy in the determination of E_f increases but in that of $\tilde{a}_f/\tilde{a}_n$ it decreases. This can be seen from the estimate

$$\frac{d\ln P_f}{dE_f} \simeq -\sqrt{\frac{a_f}{E-E_f}} = -\frac{1}{t_f}\,; \quad \frac{d\ln P_f}{da_f} \simeq \sqrt{\frac{E-E_f}{a_f}} = t_f. \tag{49}$$

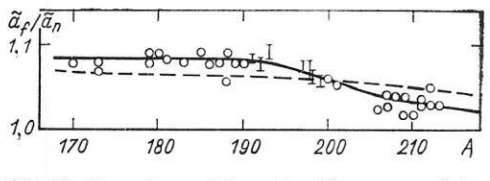

FIG. 23. Dependence of the ratio of the asymptotic level-density parameters $\tilde{a}_f/\tilde{a}_n$ on the mass number A.[62] The continuous curve shows the averaged empirical dependence, and the broken curve gives the theoretical estimate of $\tilde{a}_f/\tilde{a}_n$. The experimental values are indicated by the open circles and the vertical bars (see the text).

Very important for the determination of $\tilde{a}_f/\tilde{a}_n$ is the extension of the range of investigated energies.

Figure 23 shows the set of values obtained for the ratio $\tilde{a}_f/\tilde{a}_n$ of the level-density parameters for nuclei in which the fissility has been studied in a range of energies extending over not less than 30 MeV. For the nuclei of the transitional region Hg–Pt, Fig. 23, like all the following figures, gives values whose upper and lower bounds correspond to one of the $k^n_{\rm rot}$ assumptions indicated above. The continuous curve in Fig. 23, drawn through the experimental points, characterizes the mean empirical dependence of the ratio $\tilde{a}_f/\tilde{a}_n$ on the mass number. As already noted, the nature of this dependence is due to the existence of volume and surface components in the relations for the asymptotic level-density parameter (42). An estimate of the ratio $\tilde{a}_f/\tilde{a}_n$ based on the variations in B_s predicted by the liquid-drop model and the results of analysis of the density of the neutron resonances (see Table II) is shown in Fig. 23 by the broken curve. Overall, it agrees quite well with the experimental data but gives a weaker dependence of the ratio $\tilde{a}_f/\tilde{a}_n$ on the mass number than the empirical curve.

It should be noted that description of the fissility in all the reactions for the Pb and ^{209}Bi, ^{210}Po isotopes, i.e., nuclei with a closed shell with respect to Z or N, required reduced values of $\tilde{a}_f/\tilde{a}_n$ (Table V). At the present time it is difficult to decide whether these discrepancies reflect inadequacies of the theoretical treatment or whether they are due to certain systematic errors in the analysis of the experimental data. It is evident that both questions require further investigations, particularly in view of the appreciable discrepancy in the existing estimates of the coefficient β (see Table II).

Errors in the analysis

It is necessary to distinguish two main sources of errors in the determination of the parameters used to describe $P_f(E)$. First of all, we have that which is directly related to the measurement of the fission cross sections: the statistical error, the errors in the determination of the energy and the particle flux, the number of nuclei in the target, etc. This component of the total error δE_f hardly exceeds 0.2–0.3 MeV, as follows from the spread of the E_f values in Table V for the same compound nuclei excited in different ways. It is evidently necessary to proceed from this estimate when comparing the fission barriers of neighboring nuclei, in particular, when analyzing the isotopic dependence $E_f(Z,N)$.

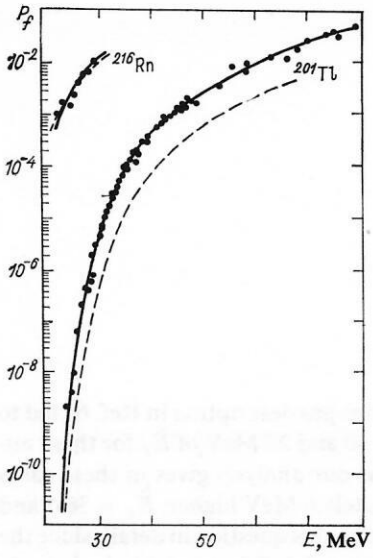

FIG. 24. Theoretical description of experimental data on the fissility of ^{201}Tl in the ^{197}Au (α, f) reaction[13,20] and of ^{216}Rn in the ^{209}Bi(^{7}Li, f) reaction.[58] Calculated curves: the continuous curve, under the assumption $k^n_{\rm rot} = 1$; the broken curve, under the assumption $k^n_{\rm rot} = \sigma^2_{1n} q(t)$ (see the text).

The error associated with the analysis itself—the imperfection of the theoretical model, the simplifying assumptions, the uncertainty of the employed parameters, etc.—can be appreciably greater than the experimental error. An important part of this error, which arises because the information about the energy dependence of $k_{\rm rot}(U)$ is inadequate, was estimated by us above on the basis of reasonable variations of the function $q(t)$. As we have noted, the total error is strongly dependent on how extensive and close to the fission threshold the fissility is studied experimentally. We give the following estimates for the total errors of the parameters in Table V:

1) $\delta(\tilde{a}_f/\tilde{a}_n) = \pm 0.01$ for sufficiently wide intervals $\Delta E \gtrsim 30$ MeV;

2) $\delta E_f = \pm (0.4–0.6)$ MeV for spherical nuclei and $\pm (0.7–1.0)$ MeV for both deformed nuclei and the transitional region of Pt–Hg.

In Fig. 24, we give results for ^{201}Tl and ^{216}Rn illustrating the errors of the analysis in favorable and unfavorable cases and ones interesting in connection with the deformation classification of nuclei in the ground state. On the basis of the formal criteria, the ^{201}Tl nucleus is usually put in the transitional group of nuclei. This is the lightest of the nuclei for which there are results of measurements of the fissility in the neighborhood of the fission threshold.[13] As for the polonium isotopes considered above (see Fig. 21), from the "bend" in the energy dependence of the ^{201}Tl fissility one can readily estimate the position of the "threshold" without recourse to any theoretical analysis: dp_f/dE below and above the point $E \sim 23$ MeV differ by not less than an order of magnitude. It can be seen that the curve of $P_f(E)$ calculated under the assumption $k^n_{\rm rot} = 1$ and $E_f = 23.6$ MeV agrees well with the experimental data up to 60 MeV, whereas the curve corresponding to the alternative possibility $k^n_{\rm rot} = \sigma^2_{1n} q(t)$ and the same threshold passes well below the experimental points. This makes it possible to conclude that the ^{201}Tl nucleus should be included in the group of spherical nuclei.[68]

Discussion of the ^{216}Rn fissility, investigated in the ^{209}Bi(^{7}Li, f) reaction,[53] is interesting from two points of view. First, Ref. 53 was a pioneering study of the effect of the collective increase in the level density on nuclear fissility. Second, ^{216}Rn is the heaviest nucleus in the interval between bismuth and radium for which it has been possible to obtain experimental data on the low-energy cross sections for fission and compound-nucleus formation. In this case, the analysis is free of many difficulties inherent in reactions with heavy ions. The continuous curve in Fig.24 corresponds to the assumption $k^n_{\rm rot} = 1$ and the parameters $E_f = 14.3$ MeV, $\tilde{a}_f/\tilde{a}_n = 1.03$; the broken curve, to $k^n_{\rm rot} = \sigma^2_{1n} q(t)$, $E_f = 12.6$ MeV, $\tilde{a}_f/\tilde{a}_n = 1.06$ (in Ref. 53, the values $E_f = 13.8$ and 13.1 MeV, respectively, are obtained for these cases). Because the investigated energy range is small, it is not possible to give preference to one variant of description over the other. Below, in Sec. 5, we shall use for ^{216}Rn the mean value $E_f = 13.5 \pm 1.0$ MeV.

Comparison of the fissility analyses

Table VI compares the data of Table V (Ref. 62) with the results of the early studies of Refs. 19 and 21, in which the

TABLE VI. Comparison of fission barriers E_f obtained by analyzing the fissility in the (α, f) and (p, f) reactions (references are indicated by square brackets).

Fissioning nucleus	E_f, MeV			Fissioning nucleus	E_f, MeV		
	[19]	[20]	[62]		[19]	[20]	[62]
^{213}At	17,0	14,3	17,3	^{191}Ir	23,7	20,6	23,2
^{212}Po	19,5	16,3	19,6	^{189}Ir	22,6	19,7	22,0
^{211}Po	19,7	17,2	20,6	^{188}Os	24,2	22,1	24,4
^{210}Po (α, f)	20,5	18,2	21,2	^{187}Os	22,7	22,2	24,8
(p, f)	21,4	—	21,2	^{186}Os	23,4	22,1	24,1
^{209}Bi	23,3	21,9	24,3	^{185}Re	24,0	24,0	26,2
^{207}Bi	21,9	19,9	22,8	^{179}Ta	26,1	25,4	28,6
^{201}Tl	22,3	19,5	23,1	^{173}Lu	28,0	27,1	30,5
^{198}Hg	20,4	19,5	21,4—22,6				

TABLE VII. Comparison of the results of different analyses of the fissility of the nuclei $^{204-208}$Pb and ^{209}Bi in the (e,f) reaction.

Fissioning nucleus	Our analysis[62]			Darmstadt[13]			Toronto[14,15]		
	E_f, MeV	a_f, MeV^{-1}	a_n, MeV^{-1}	E'_f, MeV	a_f, MeV^{-1}	a_n, MeV^{-1}	E_f, MeV	a_f, MeV^{-1}	a_n, MeV^{-1}
^{204}Pb	23.2	19.6	14.5—15.4	24.0	11.2	5.1	—	—	—
^{206}Pb	25.3	19.7	12.5—14.9	26.8	11.2	5.1	26.0	13.5	11.0
^{207}Pb	27.0	19.8	12.6—14.7	26.9	11.2	5.1	26.2	11.0	8.5
^{208}Pb	27.4	19.9	12.6—14.3	28.6	11.2	5.1	27.6	10.8	8.1
^{209}Bi	24.3	20.0	12.3—15.0	24.3	11.2	5.1	23.4	12.3	10.2

description of $P_f(E)$ did not take into account collective effects in the level density. We note that in Refs. 19, 20, and 62 either identical or well-agreeing data on the fissility in the (α,f) and (p,f) reactions (Table V) are analyzed. In Table VII, the results of Ref. 62 for the (e,f) reaction are compared with the results of the original studies of Refs. 64–66, in which the Fermi-gas model with phenomenological corrections for nucleon pairing and energy-independent parameters a_f and a_n was used to determine E_f.

In the fitting to the experimental data, the compensation of the factors absent in the model was achieved at the price of a distortion of the deduced parameters. In Ref. 20, which uses the $a_n(U)$ systematics considered at the beginning of Sec. 3, appreciably reduced values of E_f were obtained, as can be seen from Table VI. Table VII shows that by using other data one can obtain reasonable values of E_f, but then allowing values of a_f and a_n that are unjustifiably small. Note that if allowance is made for the difference between the effective, $E'_f = E_f + n\Delta_f$, and true thresholds E_f ($n = 2$ and 1 for even–even and A-odd nuclei, respectively) the agreement between our values[62] of E_f and the results of Refs. 64–66 worsens.

The superfluid model used in Ref. 19 to describe the level density made it possible to carry through the analysis to the fission threshold, and this ensured it against the appreciable inaccuracies in the value of E_f for near-magic nuclei. For such nuclei, the values of E_f obtained in Refs. 62 and 19 also agree well with the thresholds observed directly in the experiments. However, the absence of the coefficients k_{rot} in the description of the level density in Ref. 19 led to distortion of another characteristic of the fissioning nuclei—the correlation function Δ_f of the transitional states, i.e., there arose contradictions with the results of the analysis of the angular anisotropy of the fission (see Table III and Refs. 50, 57, and 68). For deformed nuclei, there is no experimental information on the fissility near the threshold, and the inadequacies of the model of Ref. 19 directly affect the values of E_f. Allowance for the collective increase in the level density leads in this case to large barrier heights compared with Refs. 19 and 20, the difference ΔE_f^{col} between them increasing with decreasing Z of the fissioning nucleus.

This last effect has a systematic nature, as we also showed by analyzing the experimental data on the fissility in the (τ,f) reaction of the lighter nuclei ^{162}Ho and ^{168}Tm,[69] which we had not considered earlier, since the measurements in Ref. 69 were made for the isolated energy $E_\tau = 44.5$ MeV. The Fermi-gas description in Ref. 69 led to the "liquid-drop" values 30 and 27 MeV of $\tilde{E}_f$ for these nuclei, respectively, whereas our analysis gives in these cases values that are approximately 6 MeV higher: $\tilde{E}_f = 36.5$ and 32.3 MeV. We have dwelt on this question in detail, since the increase in ΔE_f^{col} when the model of the level density is made more accurate has, as will be shown below, fundamental importance for conclusions about the theoretical description of experimental information on $E_f(Z,N)$.

5. THEORETICAL DESCRIPTION OF FISSION BARRIERS

Studies in which systematic microscopic calculations of the fission barriers of the preactinide nuclei by the shell-correction method have been made can be counted on one's fingers (see, for example, Refs. 70–72). It is difficult to compare them, since, as a rule, they differ in the single-particle potentials, in the parametrization of the nuclear shape, and in the description of the macroscopic component. In Fig. 25, the results of recent calculations of Pashkevich[72] are compared with the experimental values of E_f for spherical nuclei

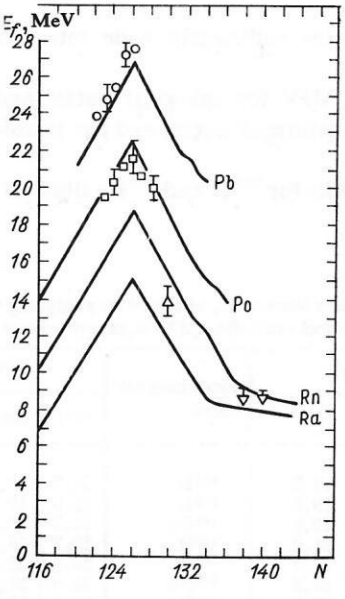

FIG. 25. Comparison of the results of microscopic calculations of E_f (continuous curves)[72] with the results of our analysis of nuclei near $N = 126$: open circles for Pb, open squares for Po, open triangles for Rn, and open inverted triangles for Ra.[56]

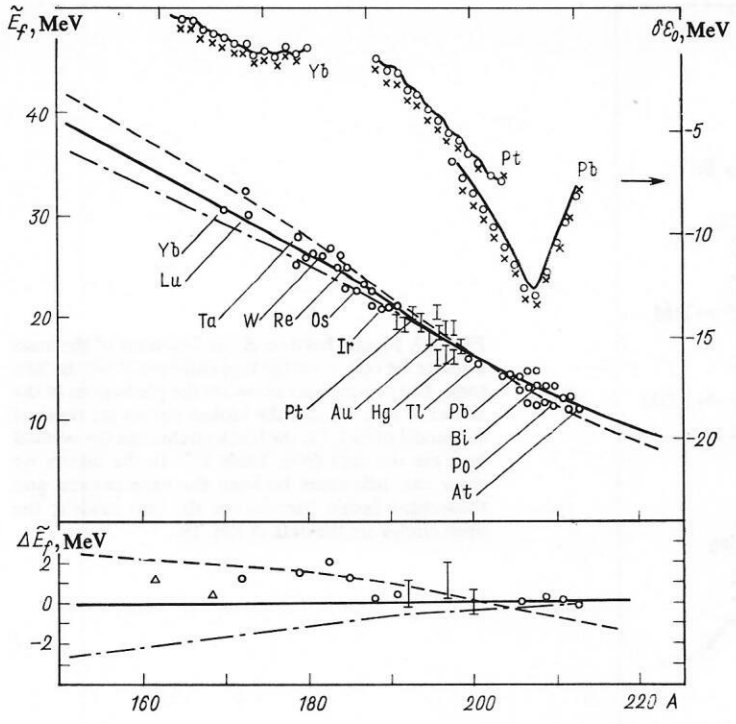

FIG. 26. Dependence of the drop component of the fission barriers $\tilde{E}_f$ on the mass number: the continuous curve represents the predictions of the liquid-drop model[15]; the broken curve, the predictions of the droplet model[73]; and the chain curve, the predictions of the model with allowance for the finite range of the effective nuclear forces.[74] The symbols for the experimental values, the open circles and the vertical bars, are as in Table V. In the upper part of the figure we show the barrier shell corrections $\delta\mathscr{E}_0$ for the corresponding models; the continuous curves are from Ref. 15, the crosses from Ref. 73, and the open circles from Ref. 74. The lower part of the figure shows the discrepancies between the predictions of the models and the experimental data for nuclei that depart from the bottom of the stability valley by not more than one neutron. The data from Table V are augmented by the values of $\tilde{E}_f$ for ^{162}Ho and ^{168}Tm (Ref. 69) in accordance with our analysis (open triangles).

in the neighborhood of the shell $Z = 82$, $N = 126$. The good agreement of the data in Fig. 25 indicates appreciable progress in the theoretical description of the fission barriers, since the discrepancies between the calculated and experimental values of E_f reached several mega-electron-volts in the early studies.

It is, however, more informative to compare the resulting barriers directly with the phenomenological description of $\tilde{E}_f(Z, N)$ in different variants of the shell model. On the one hand, it is in fact on the basis of this description that the macroscopic component of the nuclear deformation energy is calculated in the framework of the shell-correction method. At the same time, when the parameters of such a description are determined one uses not only data on the masses and quadrupole moments of the nuclei but also, as it happens, experimental information on the barriers in an assumption that is common to the fissility analysis: $\delta\mathscr{E}_f = 0$.[15,73] The question of the error of the analysis associated with it has already been discussed above and is considered in more detail in Refs. 30 and 62.

In Fig. 26 we have plotted as a function of the nucleon number A the $\tilde{E}_f = E_f - \delta\mathscr{E}_0$ values recovered from the data of Table V with the shell corrections $\delta\mathscr{E}_0$.[15] By the curves for the valley of β-stable nuclei (18) we show the variations in $\tilde{E}_f(A)$ for three widely used forms of phenomenological description of the nuclear fission barriers: the liquid-drop model (LDM),[15] the droplet model (DM),[73] and the drop model with allowance for the finite range of the effective nucleon interaction.[74] Such a comparison is correct apart from differences in the shell corrections in each of the models, but these, as is shown in the upper part of Fig. 26, are indeed small. The $\tilde{E}_f$ chains of the studied isotopes, excluding the lightest elements, cover the entire region between the curves, and therefore in the lower part of Fig. 26 we compare the experimental and theoretical information in the form of the deviations from the liquid-drop model for nuclei separated from the bottom of the β-stability valley by not more than one neutron.

All the curves in Fig. 26 pass through the interval $A = 201$–213, since to it there belong the spherical nuclei from ^{210}Tl to ^{213}At, for which the fissility has been studied to the threshold, and as a result the barrier height E_f has been determined most reliably. For the lighter nuclei, the sample of experimental data for the β-stability valley passes initially closer to the curve of the droplet model,[73] but then, for $A < 180$, deviates systematically from it, following the tendency of the curve of Krappe, Nix, and Sierk,[74] but situated above it by 2–3 MeV on the average. The deviations of the experimental values from $\tilde{E}_f^{\mathrm{LDM}}$ nowhere exceed 2 MeV.

The part played by the diffuseness of the nuclear surface and the specific energy of the interaction between the future fragments as they form at the saddle point, which are considered by the model of Ref. 74, increases with decreasing number of nucleons, and therefore a significant effect of these factors is to be expected for still lighter nuclei. The presence of the corresponding effects is indicated by analysis of the fissility of nuclei with $Z^2/A \lesssim 28$ in reactions with more energetic light particles, $E_i \gtrsim 150$ MeV,[75] and heavy ions.[76–78] It is, however, necessary to point out that instead of the effects of the finite range of the nuclear forces,[74–79] which lead to a decrease of $\tilde{E}_f$ compared with the traditional liquid-drop model,[15] one can easily take many inaccuracies of the experiment and the description of the experimental data (fission of admixtures of elements with larger Z, simplification of the level-density model, overestimation of the angular momentum transferred to the fissioning nucleus, and so forth). We

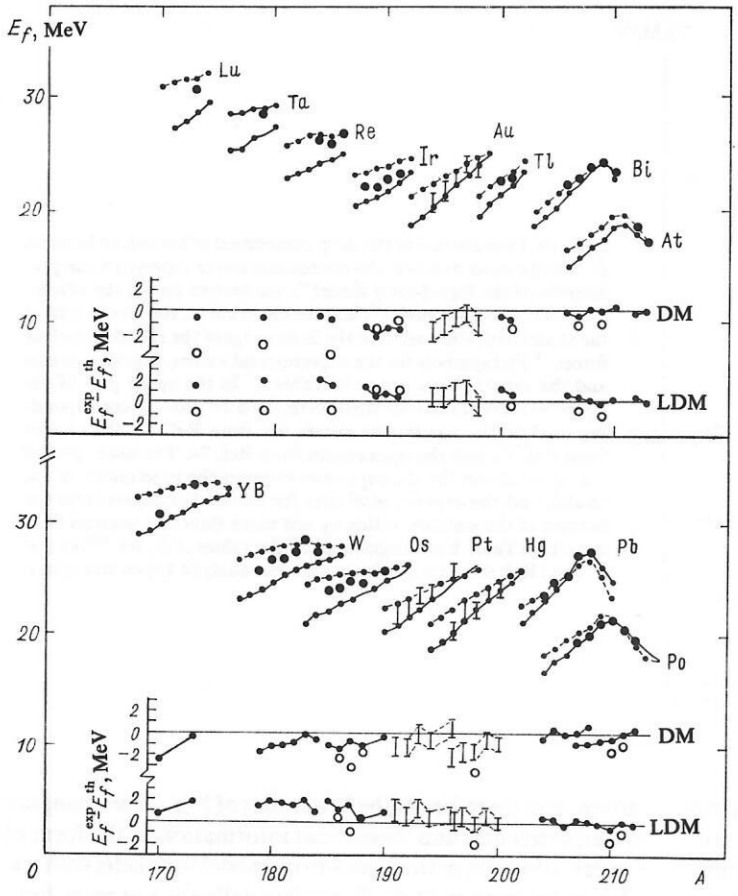

FIG. 27. Fission barriers E_f as functions of the mass number for odd Z (at the top) and even Z (at the bottom). The continuous curves are the predictions of the model of Ref. 15, and the broken curves are those of the model of Ref. 73; the black circles and the vertical bars are the data from Table V.[62] In the inserts we show the differences between the experimental and theoretical fission barriers for the two models; the open circles are the data of Ref. 19.

shall restrict ourselves to just one example from the data which we have discussed.

The data obtained in Ref. 69 on $\tilde{E}_f$ in the region of $A \sim 200$ are close to $\tilde{E}_f^{LDM}$, but for $A \sim 160$ (^{162}Ho, ^{168}Tm) they are appreciably less than E_f^{LDM} (in Fig. 26, one could not place them). This circumstance was regarded in Ref. 69 as an argument in favor of the model with allowance for the finite interaction range of the nucleons.[74] Our values of E_f for the same nuclei (triangles in Fig. 26) lie above the level $\Delta\tilde{E}_f = 0$ and differ only by (1–2)δE_f from the higher barriers of the droplet model.[73] From them there follows a quite different conclusion—neither of the descriptions of Refs. 73 and 74 is sufficiently complete.

In Fig. 27, the total barrier heights E_f are compared with the phenomenological description of the liquid-drop model[15] and the droplet model.[73] The inserts show the deviation of the experimental values E_f^{exp} from the calculated values E_f^{th} for each model. Also shown are the results discussed above (Table VI) of the analysis of the fissility in Ref. 19, which are widely used[15,73,74] to analyze the dependence $\tilde{E}_f(Z, N)$. In the considered range of Z and A, the values which we obtained for E_f are on the whole somewhat better described by the droplet model, while the isotopic dependence $E_f(Z, N)$ is, in contrast, better described by the liquid-drop model.

In the liquid-drop model, the values of $\tilde{E}_f$, expressed in the units E_S^0 of the surface energy of a spherical drop, follow a common dependence

$$\xi(x) = \tilde{E}_f/E_S^0 \tag{50}$$

on the fissility parameter

$$x = \frac{E_C^0}{2E_S^0} = \frac{c_3}{2a_2}\,\frac{Z^2}{A(1-kI^2)}, \tag{51}$$

where $E_C^0 = c_3 Z^2/A^{1/3}$ is the Coulomb energy of the spherical drop, $E_S^0 = a_2 A^{2/3}(1-kI^2)$ is the surface energy of the drop, and $I = (N-Z)/A$. In the droplet model, the ratios $E_C^0/2E_S^0$ and $\tilde{E}_f/E_S^0$ do not have such a simple property, but nevertheless in it one can find an equivalent effective fissility parameter x for the given Z and a corresponding effective value of the coefficient k. For this, we consider the isospin dependence of the parameter

$$\zeta(I^2) = \frac{2a_2}{c_3}(1-kI^2) = \frac{Z^2/A}{x}, \tag{52}$$

determining x from the transcendental equation

$$2\tilde{E}_f/E_C^0 = \xi(x)/x, \tag{53}$$

whose left-hand side contains $\tilde{E}_f$ in units of the Coulomb energy of the drop [$c_3 = 0.705$ MeV (Ref. 15)].

Figure 28a shows the dependence $\zeta(I^2)$ determined in this way for the droplet barriers,[73] and Fig. 28b shows the dependence for the experimental $\tilde{E}_f$ values obtained from the data of Table V with the shell corrections of Ref. 73. In

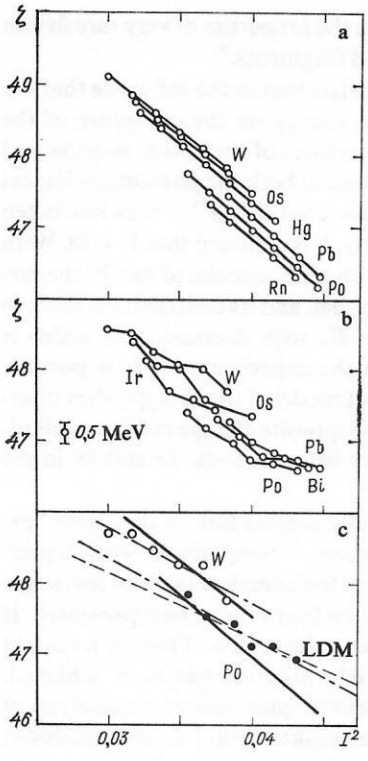

FIG. 28. Isospin dependence of the parameter $\zeta(I^2)$.[62] a) For $\tilde{E}_f$ of the droplet model[73]; b) for the experimental barriers $\tilde{E}_f$; c) data for the barriers of Po (black circles) and W (open circles) compared with the predictions of the models: continuous curve for Ref. 73 and broken curve for Ref. 15; the chain curve represents empirical fitting of k to the observed barriers.

the droplet model, ζ depends not only on the isospin I but also on Z, but for fixed Z the functions $\zeta(I^2)$ have in a narrow range of I^2 a form close to that of straight lines. The experimental data in Fig. 28b also demonstrates an analogous lamination of the lines joining the points. The observation of this effect in the experimental barriers became possible through the significant increase in the information about $E_f(Z, N)$ in Ref. 62 compared with the earlier studies.

The mean slope of the experimental $\zeta(I^2)$ chains for $Z = \text{const}$ is appreciably less than in the droplet model; this can be seen particularly clearly in Fig. 28c, in which we have retained only the $\zeta(I^2)$ values for the Po and W isotopes. The broken lines here show the predictions of the liquid-drop model with the coefficient $k = 1.78$,[15] while the continuous lines show the predictions of the droplet model, to which there correspond the effective values $k = 2.97$ for the W isotopes and $k = 3.16$ for the Po isotopes. The broken curves, fitted by the least-squares method to the experimental barriers, give the effective values $k = 2.04$ for W, 2.14 for Po, and 2.30 for the average over the five isotope chains represented in Fig. 28.

If we ignore the lamination of $\zeta(I^2)$ for different Z and analyze the complete set of the experimental data in Fig. 28, then the coefficient k will be greater than the average over the chains. It was for this reason that the study of Ref. 68, which considered a much smaller number of nuclei but in the same region of Z and N, deduced from analysis of the set of data the overestimated value $k = 2.8$, which is fairly close to the droplet model.

Thus, it follows from the analysis of the isospin dependence of the barriers that $k_{DM} > k_{exp} > k_{LDM}$ with the experimental value k_{exp} lying closer to the liquid-drop value.[15] The few studies made with heavy ions that have analyzed this dependence[80,81] also confirm the low value $k \simeq k_{LDM} \simeq 2.0$ in the considered region of nuclei. We note that in the description of Ref. 74 the coefficient is $k = 3.0$, i.e., is almost the same as in the droplet model.[73] In the more recent study of Krappe and Nix[79] it was even higher, $k = 4.0$, while the enhancement of the isospin dependence of the surface energy in the droplet model was initiated by Pauli and Ledergerber[82] ($k = 2.84$). Finally, we mention that the theoretical calculations of E_f in Ref. 72, the results of which are given in Fig. 25, were made with the parameters of Ref. 15.

The comparison of the theoretical and experimental information on the fission barriers can be summarized as follows:

1. The results of the analysis of the nuclear fissility do not confirm the tendency of the theoretical studies noted in recent years for a strong increase in the parameter of the isospin dependence of the fission barriers as compared with the description by the liquid-drop model.[15]

2. The set of data on $E_f(Z, N)$ confirms the necessity of taking into account the effects included in the modern variants of the droplet model,[73,74] but as a whole does not exhibit significant deviations from the simple liquid-drop description,[15] showing that the refinements considered in Refs. 73 and 74 affect the barrier heights in opposite directions and in a large region $A > 160$ effectively compensate each other.

6. FURTHER INVESTIGATIONS

We believe that the restrictions made in the present review on the mass and energy of the particles have not affected the completeness of our conclusions about the dependence $E_f(Z, N)$ in which we are interested. Of course, on the one hand, these restrictions greatly reduced the number of considered studies in the region of the preactinides, but, on the other hand, they made it possible to identify the experimental information whose analysis ensures the least error in the determination of the barrier heights—for E_f at the 5% level and better. Otherwise, the analysis of the data would come up against much less definite physical situations,[75,81,83] and, having greatly complicated the problem, we would not in fact have obtained anything new apart from the indications of a general nature that are fairly well known.

Study of the complete set of the accumulated data shows that in the near future too the experimental study and analysis of the energy dependence of the fissility of nuclei by light charged particles will remain the most reliable method of obtaining information about the fission barriers of the preactinides. However, to ensure advance of the experiments into the region $A < 170$, it is necessary to overcome the difficulties in obtaining targets of sufficient purity with regard to admixtures of more strongly fissioning elements. For the study of the fission of nuclei of the rare-earth group the ad-

mixture of not only Th and U is important, as in the majority of the previous studies, but also that of at least ten other elements with $Z > 70$. The method realized in Ref. 69 for investigating and taking into account the fission background of such admixtures, which uses the quadratic dependence of the kinetic energy of the fragments on the Z of the fissioning nucleus, is interesting. The estimates show that if one ensures a target purity of $\sim 10^{-5}$–10^{-6}%, then by means of particles with energy $\lesssim 100$ MeV it is possible to study the fissility and determine the height of the fission barrier in practically the entire range of nuclei, including the maximum of $E_f(Z, N)$ at $Z^2/A \sim 20$, $A \sim 100$ (see Fig. 1).

The feasibility of experimental study of the fission barriers increases appreciably with the elimination of the discrepancies between the results of the analysis of reactions with heavy ions and light charged particles.[83] Judging from the results of the latest studies (see Refs. 76–78, 84, and 85), there have been appreciable advances in this direction. The (HI, f) reactions could be a very effective tool not only for studying the isospin dependence of E_f but also for advancing into the little-studied region of nuclei with $A < 150$. Because of the dependence $V_{Coul} \sim Z_i$, one can, using (HI, f) reactions, eliminate much more readily the background of fissions of impurity nuclei with $Z > Z_t$.

Progress in the description of the (HI, f) reactions is intimately related to the extension of the experimental information (on the angular anisotropy of the fission, the cross sections of the competing processes, etc.) used in the analysis. One should think of such a step in the development of a phenomenological description of the masses and deformation energies of nuclei. Of the characteristics of the fission process, only the data on the barrier height $E_f(Z, N)$ have hitherto been used for this purpose. But precisely the data on the angular anisotropy of the fission and the effective moments of inertia $\mathscr{F}_{eff}(x)$ extracted from it have demonstrated the incompleteness of the description of the transitional configurations of a fissioning nucleus in the framework of the simple liquid-drop model.[26] The introduction in the drop model of an isospin dependence of the surface energy[15,86,87] did not overall alter though it did reduce the scale of the discrepancies with experiment.

It was shown in Refs. 27 and 88 by Strutinsky that the liquid-drop model can be significantly improved if one introduces in it a dependence of the surface tension on the curvature of the surface, this being taken into account by the parameter Γ. The value $\Gamma = -0.1$ corresponds to the theoretical curve $\mathscr{F}_{eff}^{-1}(Z^2/A)$ in Fig. 5 and, as was shown in Ref. 88, to the description of the observed fission characteristics of sufficiently strongly heated nuclei. It was recently shown in Ref. 89 that the dispersion σ_M^2 of the mass distributions of the fragments of symmetric fission in a wide range of nuclei lighter than thorium also follows the predictions of the liquid-drop model with a parameter $\Gamma \simeq -0.1$.[88] We note that the sensitivity of $\sigma_M^2(x, \Gamma)$ to the value of Γ is greater than that of the effective moment of inertia $\mathscr{F}_{eff}(x, \Gamma)$. The necessity of taking into account the factor Γ in the description of the deformation potential energy of heavy nuclei is also indicated by Ref. 90, in which an analysis is made of the experimental data on the properties of very rare fission modes with effectively cold fragments.[91]

We devote particular attention to the influence that the dependence of the surface energy on the curvature of the surface has on the characteristics of the fission process and the fissioning nucleus because in both the phenomenological descriptions which we have considered[73,74] it is not taken into account (more precisely, it is assumed that $\Gamma = 0$). With the parameter $\Gamma = -0.1$ there is associated one of the largest terms in the droplet model, and its contribution leads to an appreciable increase of E_f with decreasing Z, which is difficult to reconcile with the experiments.[92] It is possible that inclusion in the droplet model of the Krappe–Nix interaction,[79] which leads to the opposite change in E_f, can eliminate the noted discrepancy between Refs. 73 and 88 in the choice of the value of Γ.

Finally, we consider the central link in the chain "experiment → analysis of data → comparison with liquid-drop model," in which form the complete cycle of investigations of the fissility and fission barriers can be represented. It is given a prominent place in the review. There is no doubt that in this field appreciable progress has been achieved. However, not a few unresolved questions in the analysis of the data still remain. The weakest point in the employed description of the fissility is the incomplete allowance made for the weakening with the energy of the contribution of the rotational modes to the level density; in the absence of a reliable theoretical model, this weakening has been taken into account phenomenologically.

Recently, as already noted, Hansen and Jensen[61] calculated $k_{rot}(U)$ for particles placed in an oscillator potential and interacting through Elliott quadrupole–quadrupole forces. The results of Ref. 61 show that the theoretical and empirical functions $q(t) = k_{rot}(t)/k_{rot}^{adiab}(t)$ are characterized by an exponential decrease at appreciable excitations, though the calculations indicate that the weakening "sets in" much later than in Fig. 20 and that it is different for the neutron and fission channels. Is it possible to reconcile the predictions of the calculation with the experimental fissilities? This question can only be answered by further development in the theory of the collective excitations of heated nuclei and the statistical description of the fission probability. Here, we wish to draw attention to one "reserve," which may help to solve the problem.

There has recently been a revival of interest in a problem posed many years ago by Kramers,[93] who pointed out that the probability of transmission through the barrier may differ from the Bohr–Wheeler formula[1] taken as the basis of the generally adopted description of the fission width Γ_f^{BW}. The calculations of Weidenmüller *et al.*[94] show that $\Gamma_f < \Gamma_f^{BW}$ and that the difference between these widths, which is slight in the threshold region of energies, rapidly increases with increasing $E - E_f$, i.e., is qualitatively exactly as required to reconcile the calculated dependence of $k_{rot}(U)$ in Ref. 61 with the behavior of the observed fissility.

The application of new theoretical information to the analysis of nuclear fissility requires time. However, it is already possible now to draw some conclusions about possible

refinements in our knowledge of the fission barriers of the preactinides:

a) the values of E_f for spherical nuclei can hardly be changed, since their determination, as frequently emphasized, is model-independent;

b) for deformed nuclei, whose description is rather sensitively dependent on the modeling of the collective increase in the level density, the barrier heights should not change by more than 1.0–1.5 MeV;

c) the conclusions about the isospin dependence of E_f remain valid, since they are based on analysis of, not the absolute values of E_f, but only their relative variations for fixed Z for the complete set of spherical and deformed nuclei.

Completing the discussion of the directions of further work on the problem of the experimental investigation and the theoretical description of the fission barriers, it must be said that at one of its stages it will be necessary to make a "fitting" to the data for the actinides, which from the practical point of view are the most interesting nuclei though outside the scope of the present review. At the present time, the state of the investigations into the fission barriers in this region of nuclei is such that it is impossible to obtain any new information on the description of $\widetilde{E}_f(Z, N)$ from them.[95]

CONCLUSIONS

The investigations of the fission probability of the preactinide nuclei made during the last decade have made it possible to accumulate extensive experimental information on the fission barriers in the range $Z^2/A \gtrsim 28$. The main result of the significant extension of the set of studied nuclei is the establishment of the isospin dependence $E_f(N-Z, A)$. Its parameters near the β-stability valley—the region of nuclei in which reactions with light charged particles "work well"—are fairly close to the phenomenological description in the framework of the simple liquid-drop model.[15]

The development of the description of the macroscopic component of the fission barriers and the nuclear masses in these same years occurred in such a way that a step backward was made in the description of the isospin dependence. At the same time, there are weighty experimental indications in favor of the necessity of taking into account the improvements of the liquid-drop model considered by theory. In addition, the experiments shown that the developed phenomenological variants of the liquid-drop model that take into account one group of effects but ignores another are inadequate to obtain a satisfactory description of the observed dependence $E_f(Z, N)$. It is evident that the present stage is only the beginning of a major work on the creation of a theoretical formalism suitable for predicting the fission barriers in a wide range of Z and N.

Theory will be in acute need of a further extension of the experimental information, for which there are significant reserves in reactions with light charged particles and especially with heavy ions; for the study of nuclei a long way from the stability valley these reactions have no competitors. To a large degree, the progress will be determined by the possibilities of mutually consistent analysis in reactions with ions of different masses; at the present time such analysis is still far from the required state. In turn, analysis of the experimental data is required in the development of a unified description of both of the macroscopic quantities $\widetilde{E}_f$ and $\tilde{a}_f$, and also in the further development of the description of the level density and fission probability.

It is worth looking at using for the description of the fission barriers other characteristics of the fission process that are sensitive to the parameters of the liquid-drop model. Unfortunately, the present state of the experimental data in this field is such that their use is at present restricted to semiquantitative illustrations.

Very fruitful has been the second direction of investigations of the fission probability of the preactinides—the study of the statistical properties of the excited nuclei in both the equilibrium and the anomalously deformed state. In the other branches of nuclear physics it is difficult to find such striking examples of the influence on the observable characteristics of nuclei of the rearrangement of the shells with the energy, the effects of the pairing correlation of the nucleons and the associated phase transition from the superconducting to the normal state, and the part played by collective excitations in the level density—as demonstrated in the present review. The quantitative treatment shows that for the analysis of the fission probability there is no satisfactory alternative to the approach that takes into account systematically these properties of real nuclei.

[1]N. Bohr and J. Wheeler, Phys. Rev. **56**, 426 (1939).
[2]T. Ericson, Adv. Phys. **9**, 425 (1960).
[3]J. Huizenga and R. Vandenbosch, in: *Nuclear Reactions*, Vol. 2, North-Holland, Amsterdam (1962).
[4]A. Bohr, in: *Proc. of the Conf. on the Peaceful Uses of Atomic Energy*, Vol. 2, Geneva (1955), p. 220.
[5]J. A. Wheeler, in: *Fast Neutron Physics*, Part II, Interscience, New York (1963), p. 2057 (Russian translation published in: Uspekhi fiziki deleniya yader, Atomizdat, Moscow (1965), p. 7).
[6]I. Halpern and V. M. Strutinsky, in: *Proc. of the Second Conf. on the Peaceful Uses of Atomic Energy*, Vol. 15, Geneva (1958), p. 408.
[7]A. W. Fairhall, R. C. Jensen, and E. F. Neuzil, *ibid.*, Vol. 15, p. 452.
[8]C. T. Coffin and I. Halpern, Phys. Rev. **112**, 536 (1958).
[9]J. R. Huizenga, R. Vandenbosch, and R. Chaudhry, Phys. Rev. **126**, 210 (1962).
[10]J. R. Huizenga, R. Vandenbosch, and R. Chaudhry, Phys. Rev. **126**, 220 (1962).
[11]G. L. Bate, R. Chaudhry, and J. R. Huizenga, Phys. Rev. **131**, 722 (1963).
[12]D. C. Barnett, R. C. Gatti, F. Plasil *et al.*, Phys. Rev. B **134**, 952 (1964).
[13]A. Khadai-Joopari, Ph. D. Thesis, UCRL-16489, Berkeley (1966).
[14]S. G. Thompson, Ark. Fys. **36**, 267 (1967); L. G. Moretto, R. C. Gatti, and S. G. Thompson, Report UCRI-17989, Berkeley (1970).
[15]W. D. Myers and W. J. Swiatecki, Ark. Fys. **36**, 593 (1967).
[16]V. E. Viola, C. T. Roche, W. G. Meyer, and R. G. Clark, Phys. Rev. C **10**, 2416 (1974).
[17]G. M. Raisbeck and J. W. Cobble, Phys. Rev. **153**, 1270 (1967).
[18]J. B. Natowitz and E. T. Chilik, Nucl. Phys. **A172**, 1971 (1971).
[19]L. G. Moretto, S. G. Thompson, I. Routti, and R. C. Gatti, Phys. Lett. **38B**, 471 (1972); L. G. Moretto, in: *Physics and Chemistry of Fission*, Vol. 1, IAEA, Vienna (1974), p. 329.
[20]A. V. Ignatyuk, M. G. Itkis, V. N. Okolovich *et al.*, Yad. Fiz. **21**, 1185 (1975) [Sov. J. Nucl. Phys. **21**, 612 (1975)].
[21]A. V. Ignatyuk, M. G. Itkis, V. N. Okolovich *et al.*, Yad. Fiz. **25**, 25 (1977) [Sov. J. Nucl. Phys. **25**, 13 (1977)].
[22]O. A. Zhukova, A. V. Ignatyuk, M. G. Itkis *et al.*, Yad. Fiz. **26**, 473 (1977) [Sov. J. Nucl. Phys. **26**, 251 (1977)].
[23]S. D. Beĭzin, A. V. Ignatyuk, M. G. Itkis *et al.*, Izv. Akad. Nauk Kaz. SSR, Ser. Fiz.-Mat. No. 2, 3 (1977).
[24]A. V. Ignatyuk, M. G. Itkis, S. I. Mul'gin *et al.*, Pis'ma Zh. Eksp. Teor.

Fiz. **25**, 65 (1977) [JETP Lett. **25**, 58 (1977)].
[25]S. D. Beĭzin, M. G. Itkis, I. A. Kamenev *et al.*, Izv. Akad. Nauk Kaz. SSSR, Ser. Fiz.-Mat. No. 6, 54 (1983).
[26]R. F. Reising, G. L. Bate, and J. R. Huizenga, Phys. Rev. **141**, 1161 (1966).
[27]V. M. Strutinskiĭ, Yad. Fiz. **1**, 821 (1965) [Sov. J. Nucl. Phys. **1**, 588 (1965)].
[28]K. G. Kuvatov, V. I. Okolovich, and G. N. Smirenkin, Pis'ma Zh. Eksp. Teor. Fiz. **8**, 277 (1968) [JETP Lett. **8**, 171 (1968); K. G. Kuvatov, V. N. Okolovich, L. A. Smirina *et al.*, Yad. Fiz. **14**, 79 (1971) [Sov. J. Nucl. Phys. **14**, 45 (1972)].
[29]C. M. Perey and T. G. Perey, At. Nucl. Data Tables **17**, No. 1 (1976).
[30]A. V. Ignatyuk, M. G. Itkis, I. A. Kamenev *et al.*, Yad. Fiz. **40**, 625 (1984) [Sov. J. Nucl. Phys. **40**, 400 (1984)].
[31]R. K. Chaudhury, G. Rekhe, and S. S. Kapoor, Phys. Rev. C **22**, 1360 (1980).
[32]V. S. Bychenkov, V. D. Dmitriev, A. I. Obukhov *et al.*, Yad. Fiz. **30**, 30 (1979) [Sov. J. Nucl. Phys. **30**, 16 (1979)].
[33]A. V. Malyshev, *Plotnost' urovneĭ i struktura atomnykh yader* (*Level Density and Nuclear Structure*), Atomizdat, Moscow (1969).
[34]A. Gilbert and A. Cameron, Can. J. Phys. **43**, 1446 (1965); P. Braweazio and A. Cameron, Can. J. Phys. **47**, 1029 (1969).
[35]A. V. Ignatyuk and V. S. Stavinskiĭ, Yad. Fiz. **11**, 1213 (1970); A. V. Ignatyuk, V. S. Stavinskiĭ, and Yu. N. Shubin, in: *Nuclear Data for Reactors*, Vol. 2, IAEA, Vienna (1970), p. 889.
[36]V. M. Strutinskiĭ and V. M. Kolomiets, in: *Materialy 8-ĭ zimneĭ shkoly LIYaF po fizike yadra (Proc. of the Eighth Winter School of the Leningrad Institute of Nuclear Physics on Nuclear Physics)*, Vol. 2, USSR Academy of Sciences, Leningrad (1973), p. 483.
[37]A. Bohr and B. R. Mottelson, *Nuclear Structure*, Vol. 2, Benjamin, Reading, Mass. (1975) (Russian translation published by Mir. Moscow (1977)).
[38]A. V. Ignatyuk, G. N. Smirenkin, and A. S. Tishin, Yad. Fiz. **21**, 485 (1975) [Sov. J. Nucl. Phys. **21**, 255 (1975)].
[39]N. A. Perfilov, in: *Physics and Chemistry of Fission*, Vol. 2, IAEA, Vienna (1965), p. 283.
[40]A. V. Ignatyuk, Yad. Fiz. **21**, 20 (1975) [Sov. J. Nucl. Phys. **21**, 10 (1975)]; *Materialy 13-ĭ zimneĭ shkoly LIYaF po fizike yadra (Proc. of the 13th Winter School of the Leningrad Institute of Nuclear Physics on Nuclear Physics)*, Vol. 2, USSR Academy of Sciences, Leningrad (1978), p. 33.
[41]A. I. Vdovin, V. V. Voronov, L. A. Malov *et al.*, Fiz. Elem. Chastits At. Yadra **7**, 952 (1976) [Sov. J. Part. Nucl. **7**, 380 (1976)].
[42]A. V. Ignatyuk, K. K. Istekov, and G. N. Smirenkin, Yad. Fiz. **29**, 875 (1979) [Sov. J. Nucl. Phys. **29**, 450 (1979)].
[43]A. V. Ignatyuk and Yu. N. Shubin, Izv. Akad. Nauk SSSR, Ser. Fiz. **37**, 1947 (1975).
[44]R. Batchelor, W. Gilboy, and J. Towle, Nucl. Phys. **65**, 236 (1965); R. Owens and J. Towle, Nucl. Phys. **A112**, 337 (1968).
[45]D. Hill and J. Wheeler, Phys. Rev. **89**, 1125 (1953).
[46]G. Sauer, H. Chandra, and U. Mosel, Nucl. Phys. **A264**, 221 (1976).
[47]J. Tüke and W. J. Swiatecki, Nucl. Phys. **A372**, 149 (1980).
[48]T. Dossing and A. S. Jensen, Nucl. Phys. **A222**, 493 (1974); J. R. Huizenga, A. N. Behkami, J. S. Sventek, and R. W. Atcher, Nucl. Phys. **A223**, 577 (1974).
[49]A. V. Ignatyuk and Yu. V. Sokolov, Yad. Fiz. **19**, 1229 (1974) [Sov. J. Nucl. Phys. **19**, 628 (1974)].
[50]A. V. Ignatyuk, K. K. Istekov, and G. N. Smirenkin, Yad. Fiz. **36**, 54 (1982) [Sov. J. Nucl. Phys. **36**, 32 (1982)].
[51]L. G. Moretto, R. S. Gatti, S. G. Thompson *et al.*, Phys. Rev. **178**, 1845 (1969).
[52]M. G. Itkis, K. G. Kuvatov, V. N. Okolovich *et al.*, Yad. Fiz. **16**, 258, 1150 (1972) [Sov. J. Nucl. Phys. **16**, 144, 631 (1973)].
[53]S. Nilsson, C. Jang, A. Sobiczewski *et al.*, Nucl. Phys. **A131**, 1 (1968).
[54]V. G. Ippolitov, Yu. A. Nemilov, Yu. A. Selitskiĭ, and V. B. Funshteĭn, Yad. Fiz. **14**, 939 (1971) [Sov. J. Nucl. Phys. **14**, 526 (1972)].
[55]H. C. Britt and J. R. Huizenga, Phys. Rev. C **9**, 435 (1974).
[56]Yu. A. Selitskiĭ, Fiz. Elem. Chastits At. Yadra **10**, 314 (1979) [Sov. J. Part. Nucl. **10**, 121 (1979)].
[57]A. V. Ignatyuk, K. K. Istekov, and G. N. Smirenkin, Yad. Fiz. **30**, 1205 (1979) [Sov. J. Nucl. Phys. **30**, 626 (1979)]; A. V. Ignatyuk, K. K. Istekov, V. N. Okolovich, and G. N. Smirenkin, in: *Physics and Chemistry of Fission*, Vol. 1, IAEA, Vienna (1980), p. 421.
[58]H. Freiesleben, H. C. Britt, and J. R. Huizenga, in: *Physics and Chemistry of Fission*, Vol. 1, IAEA, Vienna (1974), p. 447.
[59]H. Hagelund and A. S. Jensen, Phys. Scr. **15**, 225 (1977).
[60]P. A. Gottschalk and T. Ledergerber, Nucl. Phys. **A278**, 16 (1977).
[61]G. Hansen and A. S. Jensen, in: *IAEA Advisory Group Meeting on Basic and Applied Problems of Nuclear Level Densities*, BNL-NCS-51694, Upton (1983), p. 161.
[62]A. V. Ignatyuk, M. G. Itkis, I. A. Kamenev *et al.*, Yad. Fiz. **40**, 1404 (1984) [Sov. J. Nucl. Phys. **40**, 892 (1984)]; Preprint 5-84 [in Russian], Kazakh Institute of Nuclear Physics, Alma-Ata (1984).
[63]D. Türck, W. Ziga, and H. G. Clerck, Phys. Lett. **49B**, 335 (1974).
[64]D. Türck, H. G. Clerck, and H. Trager, Phys. Lett. **63B**, 203 (1976).
[65]T. E. Drake, L. Pai, and I. Nascimento, Nucl. Phys. **A259**, 317 (1976).
[66]A. Kernohan, T. E. Drake, A. Chung, and L. Pai, Phys. Rev. C **16**, 239 (1977).
[67]J. Moffatt and D. Reitmann, Nucl. Phys. **65**, 130 (1965).
[68]A. V. Ignatyuk, K. K. Istekov, and G. N. Smirenkin, Yad. Fiz. **32**, 347 (1980) [Sov. J. Nucl. Phys. **32**, 180 (1980)].
[69]F. D. Becchetti, K. H. Hicks, C. A. Fields *et al.*, Phys. Rev. C **28**, 1217 (1983).
[70]U. Mosel, Phys. Rev. C **6**, 971 (1972).
[71]P. Möller and J. P. Nix, Nucl. Phys. **A229**, 269 (1974).
[72]V. V. Pashkevich, in: *Mezhdunarodnaya shkola-seminar po fizike tyazhelykh ionov* (*International Seminar School on Heavy-Ion Physics*), JINR, Dubna (1983), p. 405.
[73]W. D. Myers, *Droplet Model of Atomic Nuclei*, IFI/Plenum, New York (1977).
[74]H. J. Krappe, J. P. Nix, and A. J. Sierk, Phys. Rev. C **20**, 992 (1979).
[75]S. A. Il'inov, E. A. Cherepanov, and S. E. Chigrinov, Yad. Fiz. **32**, 322 (1980) [Sov. J. Nucl. Phys. **32**, 166 (1980)].
[76]M. Blann and T. T. Komoto, Phys. Rev. C **26**, 472 (1982).
[77]S. D. Beĭzin, M. G. Itkis, Yu. A. Muzychka *et al.*, Yad. Fiz. **39**, 1093 (1984) [Sov. J. Nucl. Phys. **39**, 689 (1984)]; Preprint R7-83-482 [in Russian], JINR, Dubna (1983).
[78]J. Vander Plicht, H. C. Britt, M. M. Fowler *et al.*, Phys. Rev. C **28**, 2022 (1983); H. C. Britt, in: *Mezhdunarodnaya shkola-seminar po fizike tyazhelykh ionov* (*International Seminar School on Heavy-Ion Physics*), JINR, Dubna (1983), p. 381.
[79]H. J. Krappe and J. R. Nix, in: *Physics and Chemistry of Fission*, Vol. 1, IAEA, Vienna (1974), p. 159.
[80]M. Dahlinger, D. Vermeulen, and K. H. Schmidt, Nucl. Phys. **A376**, 94 (1982).
[81]S. D. Beĭzin, M. G. Itkis, Yu. A. Muzychka *et al.*, Yad. Fiz. **37**, 809 (1983) [Sov. J. Nucl. Phys. **37**, 482 (1983)].
[82]H. C. Pauli and T. Ledergerber, Nucl. Phys. **A175**, 545 (1971).
[83]A. V. Ignatyuk and G. N. Smirenkin, in: Mezhdunarodnaya shkola-seminar po fizike tyazhelykh ionov (International Seminar School on Heavy-Ion Physics), JINR, Dubna (1983), p. 389.
[84]S. E. Vigdor, H. Z. Karwovski, W. E. Jacobs *et al.*, Phys. Rev. C **26**, 1035 (1982).
[85]H. J. Karwovski and S. E. Vigdor, Phys. Rev. C **29**, 872 (1984).
[86]S. Cohen and W. J. Swiatecki, Ann. Phys. (N.Y.) **22**, 406 (1963).
[87]W. D. Myers and W. J. Swiatecki, Nucl. Phys. **81**, 1 (1966).
[88]V. M. Strutinskiĭ, Zh. Eksp. Teor. Fiz. **45**, 1900 (1963) [Sov. Phys. JETP **18**, 1305 (1964)].
[89]E. N. Gruzintsev, M. G. Itkis, V. N. Okolovich *et al.*, Yad. Fiz. **39**, 1336 (1984) [Sov. J. Nucl. Phys. **39**, 844 (1984)]; Z. Phys. A **316**, 61 (1984).
[90]R. W. Hasse, J. Treiner, and P. Schuk, "*New ideas on the fission process*," *Invited paper at the Sixth Conf. on Neutron Physics*, Kiev (1983).
[91]M. Montaya, J. Phys. **44**, 785 (1983); C. Signarbieux, M. Montaya, and M. Ribrag, J. Phys. Lett. **42**, 487 (1981).
[92]R. W. Hasse, Ann. Phys. (N. Y.) **68**, 377 (1971).
[93]H. A. Kramers, Physica **7**, 284 (1940).
[94]P. Grangé and H. A. Weidenmüller, Phys. Lett. **96B**, 26 (1980); P. Grangé, Li Jun-Qing, and H. A. Weidenmüller, Phys. Rev. C **27**, 2063 (1983).
[95]S. Bøjrnholm and J. E. Lynn, Rev. Mod. Phys. **52**, 725 (1980).

Translated by Julian B. Barbour